RESEARCH ARTICLE

A Computational Study of Magneto-Convective Heat Transfer Over Inclined Surfaces With Thermodiffusion

MUHAMMAD FAWAD KHAN[ID]1, **MUHAMMAD SULAIMAN**[ID]1, **ADDISU NEGASH ALI**[ID]2, **GHAYLEN LAOUINI**[ID]3, **FAHAD SAMEER ALSHAMMARI**[ID]4, **AND MAJDI KHALID**[ID]5

[1]Department of Mathematics, Abdul Wali Khan University, Mardan 23200, Pakistan
[2]Faculty of Mechanical and Industrial Engineering, Bahir Dar Institute of Technology, Bahir Dar University, Bahir Dar, Ethiopia
[3]College of Engineering and Technology, American University of the Middle East, Egaila 54200, Kuwait
[4]Department of Mathematics, College of Science and Humanities in Al-Kharj, Prince Sattam bin Abdulaziz University, Al-Kharj 11942, Saudi Arabia
[5]Department of Computer Science, College of Computers and Information Systems, Umm Al-Qura University, Makkah 21955, Saudi Arabia

Corresponding author: Addisu Negash Ali (addisuan@gmail.com)

ABSTRACT In this article, the ocean energy generator system is analysed. The need for sustainable renewable energy systems is continually growing, given the situation of the world's energy supplies. Numerous similar systems, including photovoltaic solar collectors, biomass, and wind turbines are used for energy generation. The ocean energy generator system uses the magnetohydrodynamics transformation concept to convert kinetic energy to electrical energy. Similar to conventional generators, an ocean generator requires an applied magnetic field to generate current, making it a critical component of the system. To optimize the performance and efficiency of ocean generators, various devices utilizing superconducting magnets have been developed, including Hall current generators, rotating channels, rotating disc magnetohydrodynamics generators, and helicoid generators. However, these systems also involve complex heat, momentum, and mass transfer, which can be better understood through mathematical modeling. The similarity transformation are introduced to transform the mathematical model from partial differential equation system to ordinary differential equation system. By adopting this approach, the numerical solution is significantly simplified while still preserving numerous crucial physical aspects of the studied heat and material transport phenomena. The physical characteristics of sea waves are governed by the three variables of seawater: temperature, salinity, and pressure. Small dispersed particles also affect the generation of hydroelectric power from surface water. The behaviour of velocity, temperature, and salinity profile is observed for the variations of different parameters such as magnetic, Grashof number and heat source. The system is converted into an optimization problem and solved by a neural network procedure. The solutions are compared with reference solutions for validation. The errors, performance, testing and training data are also presented graphically. The data is typically visualized using histograms, line graphs, and other visual aids. This allows for easier comprehension and analysis of the data.

INDEX TERMS Computational analysis, magnetic field, energy generator, nonlinear systems, dynamic parameters, neuro-computing, hybridization, heat transfer, machine learning.

I. INTRODUCTION

Many different types of sustainable and renewable energy systems can be used to generate electricity or power homes,

The associate editor coordinating the review of this manuscript and approving it for publication was Qi Zhou.

businesses, and communities. Some common examples include Solar photovoltaic (PV) systems, which use panels to convert sunlight into electricity, Wind turbines, which generate electricity from the wind, Hydroelectric power plants, which use the movement of water to generate electricity, Biomass energy systems, which burn organic materials like

wood or crops to generate electricity, Geothermal energy systems, which use heat from the Earth to generate electricity. The need for sustainable renewable energy systems is continually growing, given the situation of the world's energy supplies. Numerous similar systems, including photovoltaic solar collectors, [1], wind turbines [2], recharged geothermal reservoirs [3], and biomass [4], [5], have been invented and enhanced. There has also been much interest in marine energy systems, especially in Asia. Thermal energy conversion in the ocean, tidal power plants [6], [7], and wave energy conversion devices [8] are just a few reliable methodologies that have been developed. The MHD (magneto-hydrodynamic) saltwater generator is a very intriguing and practical endeavour, although other alternative marine renewable concepts have been put forth.

The device utilizes the MHD principle to transform kinetic energy into electrical energy. The kinetic energy is obtained from ocean/tidal current [9]. As a conventional generator, the applied magnetic field is also an important factor in an ocean generator. In terms of optimizing the performance and efficiency of ocean generators. Many devices are described such as Hall current generators [10], [11], rotating channels [12], [13], rotating disk MHD generators [14], and helicoid generators exploiting super-conducting magnets [15], [16]. Different characteristics, such as heat, momentum, and mass (salinity) transport, are intricate in these systems. These characteristics are enhanced in mathematical and computational modelling. Seawater has three properties (temperature, salinity, and pressure) which quantify the velocity of sea waves physically. Small dispersed particles also affect hydro-electricity generation from surface water [17], [18]. Khan et al studied nanofluid flow of Maxwell model over a vertical plate extending infinitely with ramped and isothermal wall temperature and concentration [19], [20]. Researchers have recently paid attention to inclined magneto-fluid dynamic flow with and without mass and heat transfer. Numerous multi-physical factors relevant to energy generation systems have been considered in these studies. Srikanth et al. [21] examined how radiative flux affected the convection flow of magnetised nano-fluid from a porous inclined plate. A study conducted by Ramesh et al. about the properties of momentum and heat transfer in a hydro-magnetic flow of dusty fluid over a stretched sheet that is inclined and has an imbalanced heat source and sink, where the flow is caused by a linear stretching of the sheet [22]. A stretched plate's boundary layer flows in a fluid-particle suspension. According to Kabir and Al Mahbub [23], using the Nachtsheim-Swigert shooting iteration technique and a sixth order Runge-Kutta integration scheme, the effect of thermophoresis on an unsteady magneto-hydrodynamic (MHD) free convection flow over an inclined porous plate with time-dependent suction in the presence of a magnetic field and heat generation has been taken into consideration. Palani and Kim report the MHD free convection flow across a semi-infinite inclined plate exposed to a fluctuating surface temperature is investigated numerically.

The energy equation considers the effects of Joule heating and viscous dissipation [24], [25]. Ramadan and Chamkha in [26] did a numerical study on the issue of constant, laminar, free convection flow of a particulate suspension across an infinite, permeable, inclined, and isothermal flat plate when a transverse magnetic field is present and affects of fluid heat absorption are present. Most two-phase models do not take into consideration the impacts of viscous particle flow. Wang and Chen reported in [27] and [28], to study the boundary layer flow (BLF) due to mixed convection over an inclined wavy plate having transverse magnetic flux, the implicit approaches spline alternating-direction and coordinate system transformation are implemented. They also found that the flow about leading brink over the wavy surface accelerates as magnetic body force rises. On the other hand, the flow slows down further away from the leading edge. The non-iso-solutal and non-isothermal hydromagnetics free convection properties of Joule and viscous dissipation from a porous inclined surface were explored by Chen [27].

The research mentioned above mostly disregarded simultaneous species diffusion (mass transfer). Although, salinity is a severe problem in study of MHD ocean generators. In such transport devices, it is crucial to study the mass transfer, and heat transfer in combined form [9], [29]. Following the Fickian law [30], mass diffusion adds certain complicated traits to mixed convection flows. Rashidi et al. considered viscous, laminar mixed convection BLF across a horizontal wall coupled with a chemical reaction. The controlling equations are written in dimensional-less form. Group theory is used to find these equations' invariant solutions under a certain continuous one-parameter group. The differential transform method is then used to get series solutions for the velocity, temperature, and concentration functions of the transformed coupled system of equations [31], and Ferdows et al. [32] analyse heat and mass transportation on moving nano-porous wall in porous media with hydrodynamic and concentration-dependent diffusivity, thermal slip boundary conditions, accounting for the Soret and Dufour effects, and viscosity depend on temperature. The research of Zueco et al. [33] is fascinating, in which a mathematical model that describes the heat and mass transfer of an electrically conducting fluid across a perforated horizontal surface in the presence of Joule (Ohmic) heating and viscous. The impact of chemical reactions and entropy on Darcy-Forchheimer flow, involving H_2O and $C_2H_6O_2$ along with magnetised nanoparticles, is being investigated for its significance in [34], [35], and [36]. Makinde [37] employed network modelling to examine varying thermo-physical effects in thermophoretic magneto-convection. Although, many investigations do not consider Soret and Dufour. Intending to assess the combined impacts of heat and mass transfer in laminar boundary layer flows in forced, and natural convection can be complex and require the use of advanced numerical techniques to predict accurately. Under the supposition that constitutive equations for the heat and mass fluxes of diluted solutes follow linear

forms in accordance with the thermodynamics of irreversible processes, momentum, energy, and mass balance equations are simultaneously solved by Abreu et al. [38]. Examining Non-Linear Convective Heat Transfer through a Hybrid Heuristic-Driven Neural Soft Computing Model: A Quantitative Study [39], [40], [41]. T Gul reports flow of a hybrid nanofluid with radiative couple stress over an inclined stretching surface under the influence of non-linear convection and slip boundary effects [42]. F Khan investigates unipolar electrohydrodynamic pump flow using a hybrid metaheuristic novel approach based on neurocomputing [43]. Theoretical research was offered to look at the peristaltic pumping of nanofluids over a deformable channel with double-diffusive convection (thermal and concentration diffusive). The need to investigate the impact of nanofluid dynamics flow of fluids and solids through the body in biological vessels as shown by the movement of waste products, food molecules, hormones, ions and heat during blood circulation motivated the development of the model and fraction blood flow [44], [45], [46], [47], [48]. Using Mathematica, Anwar Bég and Tripathi showed the significant impact, over peristaltic propulsion, thermo-diffusion in deformable channels [49], [50], [51], [52]. A Triboelectric Nanogenerator with Guided-Liquid Hybrid Design for Efficient and Omnidirectional Energy Harvesting from Ocean Waves study is reported in [53]. Moreover, many studies discussed the complex interaction between wave amplitude, Soret and Dufour effects, and buoyancy forces. Numerous studies have been published assessing the cross-diffusion impact on double-diffusive BLF. Such as the Graetz problem study by Coelho and Telles [54] in which Soret and Dufour effects are considered while analysing simultaneous heat and mass transmission between parallel surfaces. Consideration is given to axial, transverse, and longitudinal advection, heat and mass transfer, and the MHD Sakiadis flow in porous media research by Anwar et al. [55]. T Gul et al. investigate the heat transfer efficiency of nanofluids made from graphene oxide flowing in an upright channel through a permeable medium [56]. Anwar Bég et al. [57] implement a variational finite element (VFE) approach for examination of cross-diffusion and micromorphic flow, taking porous medium into account. In porous media, Vasu et al. looked into the effects of Soret and Dufour on the hydromagnetic transport from a spherical body. The effects of mass flux, in dynamic laminar gas flow, on cross-diffusion (Soret-Dufour) were also addressed by Vasu et al. [58] with robust finite difference solutions. G Yao discussed principles and control strategy of an innovative wave-to-Wire system with embedded optimization for Ocean energy storage [59]. RN Silva investigate conceptual design of a combined energy conversion system that utilizes both ocean currents and waves, and is implemented on a single platform. The system, named as Tidal-Waves Generator [60]. According to these studies, due to the existence of density variation in flow, the effects of soret of dufour are essential. These studies have also highlighted that when heat transfer and mass transfer happen

simultaneously in a moving fluid, energy flux is created that is caused by concentration gradients and temperature gradients ("composition gradients"). In [61], the SCA-SQP-ANN technique was utilized to conduct a numerical investigation of the heat transfer and boundary layer flow in the MHD Falkner-Skan equation, which is caused by a symmetric dynamic wedge. The Dufour effect refers reciprocal process of Soret effect. It is energy that has transferred that difference in concentration causes. The Soret or thermo-diffusion effect is the mass transportation caused by variation in temperature; it is a form of passive transport from one side of the membrane to another.

The above investigations did not consider plate inclination in MHD flow with thermo-diffusion and heat production effects. This work investigates the impacts of heat production and the transport phenomena in an MHD ocean generator by means of a thermo-diffusion experiment in which particles are injected into an inclined surface at a rate that depends on both temperature and the inclination angle. Due to inclusion of Soret effect, it has a significant role in transport phenomena in saltwater solutions. With heat production presents a steady-state model for seawater flow down over inclined non-conducting plate that exhibits magnetohydrodynamic double-diffusive convection. In order to simulate an ocean energy generator, we first considered the governing equations of the system. These equations can be written in a form that is easily adapted to this purpose. Then, it will convert into a system of coupled equations, and then show that several thermodynamic parameters control the coefficients in these equations, including the plate inclination,, the Grashof number (G_r), a heat source parameter ($\bar{\alpha}$), the modified Prandtl number (P_s), the Prandtl number (P_r), the Soret number (S_r) and magnetic body force parameter (M).

The salient features of this work are categorically given below:

- The ocean energy generator is considered under the effect of Soret effects, which has a significant role in saltwater.
- The impacts of heat production and thermo-diffusion on the transportation over a surface with some inclination in an MHD ocean energy generator.
- The model is transformed into an optimization problem.
- For solving the model NN-LMA technique is employed.
- The solution of model is found in the form of surrogate solutions.

The rest of paper is organized as follows: section II - Formulation of mathematical model: this section presents formulation of mathematical model; section III - Transformation of the model; discusses the transformation of model to a system of ordinary differential equations; section IV - Methodology - this section describes the research design, including the methods used to collect and analyze data, section V - Computational Experimentation: this section will present the findings of the research, including any statistical analysis or data visualization, results and explain their significance in
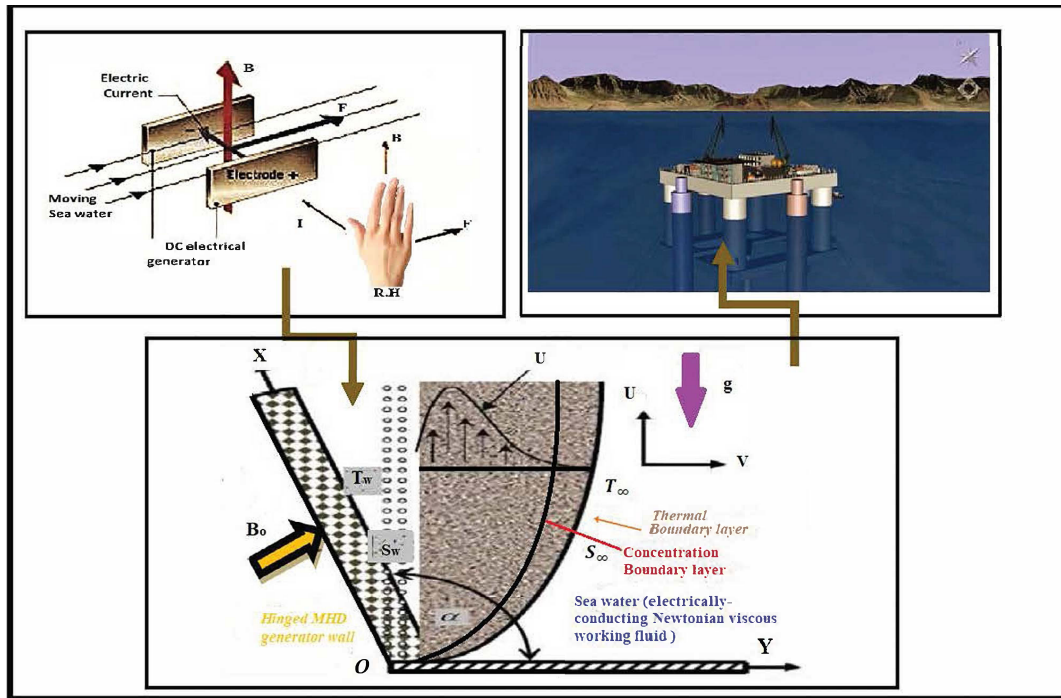
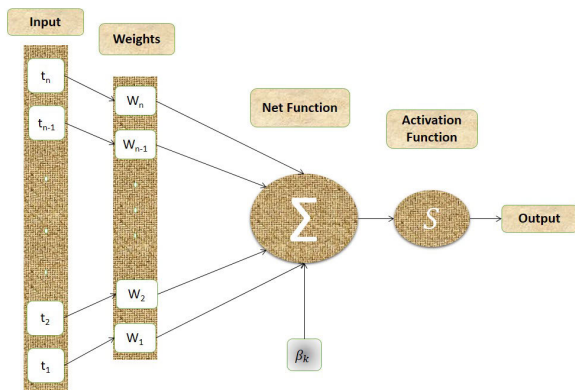**FIGURE 1.** Model of ocean magnetic energy generator.

FIGURE 2. Structure of nodes of ANN.

relation to the research question and literature review and section VI - conclusions: this section will summarize the main findings and implications of the research, and suggest future research directions.

II. FORMULATION OF MATHEMATICAL MODEL

Ocean thermal energy conversion (OTEC) systems offer humanity a workable future. Engineers from Russia, France, the United States, and Japan have all done numerous ground-breaking studies into this type of renewable energy. The basic idea of ocean energy generator with seawater as a functioning fluid is summarised by a potential design with the coordinate system in Figure 1. Seawater is considered a functioning fluid in the basic idea of energy production by ocean generators. The near-wall flow in these systems is considered in simple two-dimensional form. The boundary layer flow is upward along the X-axis, which is directed along

the generating channel plate; the Y-axis is inclined to it. The inclination angle, α, is indicated here. At first, it is considered that the temperature for plate and fluid, i.e. (T_∞) and salinity (S_∞) throughout the fluid. The dynamic wall moves over X-direction having constant velocity, and it is further considered that the wall of generator channel, i.e. plates and fluid, is in rest position. Gradually, the temperature of the plate increased to T_w ($> T_\infty$) and, similarly, species salinity is increased to S_w ($> S_\infty$), and the values are maintained subsequently. The temperatures over the wall are denoted by T_w, and rate of salt, i.e. species salinity over wall S_w and T_∞, S_∞, which denote these quantities at ends of the wall [30]. Hall currents, energy conversion of a fluid flow into heat due to the friction between fluid layers (viscous dissipation) and heating of a material due to the flow of an electrical current (Joule (Ohmic) heating) are not taken into consideration. While a weak magnetic field is considered. In the direction of Y, the intensity of applied magnetic is B_o. The applied magnetic field is always at a right angle to the wall. Whenever a magnetic field is applied, it is directed away 90° about the plate. As a result, the magnetic field does not change orientation, but the wall can. In relation to a wall, the Lorentz force always moves in the same direction (plate). For the mathematical equations of continuity, conservation of momentum, species (salinity) conservation, and conservation of energy, which includes heat production and thermal diffusivity effects, can be demonstrated to take the following with boundary layer approximation and Boussinesq assumptions:

$$\frac{\partial U}{\partial X} + \frac{\partial V}{\partial Y} = 0 \tag{1}$$

$$\left(U \frac{\partial U}{\partial X} + V \frac{\partial U}{\partial Y} \right) = \nu \left(\frac{\partial^2 U}{\partial Y^2} \right) + g\beta \left(T - T_\infty \right) \sin \alpha$$
$$- \frac{\sigma B_o^2}{\rho} U \qquad (2)$$

$$\left(U \frac{\partial S}{\partial X} + V \frac{\partial S}{\partial Y} \right) = K_s \left(\frac{\partial^2 S}{\partial Y^2} \right) + F_s \left(\frac{\partial^2 T}{\partial Y^2} \right) \qquad (3)$$

$$\left(U \frac{\partial T}{\partial X} + V \frac{\partial T}{\partial Y} \right) = K_T \left(\frac{\partial^2 T}{\partial Y^2} \right) + \frac{Q_T}{\rho C_p} \qquad (4)$$

The associated BCs are:

$$\text{At } Y = 0 : U = V = 0; T = T_w = T_\infty + \sin \alpha;$$
$$S = S_w = S_\infty + \sin \alpha \quad As \quad Y \to \infty :$$
$$U \to 0, \quad V \to 0, \ T \to T_\infty, S \to S_\infty \qquad (5)$$

here, the magnetic field strength is B_0, and the kinematic viscosity (fluid's internal resistance) is ν. The constants represent the thermal diffusivity caused by salinity $K_s = K/\rho C_s$ and temperature $K_T = K/\rho C_s$, respectively. The diffusion rate of molecule (thermal diffusion coefficient) is F_s. Under constant pressure, the specific heat is C_p, uniform velocity is denoted by U, the electric conduction of fluids is σ, and the acceleration brought on by gravity is g. The mass expansion coefficient is *beta** while the volume expansion (thermal) coefficient is β. $Q_T = (T - T_\infty) Q^*$ represents heat production, while fluid density is denoted by ρ. It is significant to notice that equation enforces thermal and solid boundary requirements equation (5) adheres to Gebhart's et al. [30] technique and represents the involvement of wall direction on the solutal (species concentration) fields and temperature. Despite this, they are neither non-isothermal nor non-isosolutal because the streamwise coordinates remain constant. Although it is not taken into consideration in the current study, this could offer future model development. Particularly in MHD ocean generator conditions, it is impossible to entirely regulate thermal and species impacts at the wall. With the existing fluid dynamics methods, imitating the whole spatial or temporal variety of such processes is impossible. Some logical and verified assumptions must be taken to construct a solid boundary value problem. These assumptions are based on boundary-layer theory in accordance with Gebhart [30]. This offers a credible estimation of the phenomena of near-wall transport. Analytical solutions are not possible for the BVP posed by the Eqs (1)-(4) under BCs (5). Numerical solutions are the sole practical choice for primitive variables. In terms of significant dimensionless variables, even numerical methods to the fundamental boundary value problem, including those based on finite elements or finite differences, fail to solve the problem. The problem is then made dimensionless by adding similarity transformations, which convert the mathematical model from a partial differential equation (PDE) to a system of ordinary differential equations (ODE). This keeps many crucial physical elements of the transport phenomenon under research while considerably simplifying the numerical solution.

III. TRANSFORMATION OF MODEL
Defining the dimensionless variables before continue with the analysis is as follows:

$$\eta = y\sqrt{\frac{U_0}{2\nu X}},$$
$$\psi = \sqrt{2\nu U_0 X} f(\eta),$$
$$\theta = \theta(\eta) = \frac{T - T_\infty}{T_w - T_\infty}, \quad \phi = \phi(\eta) = \frac{S - S_\infty}{S_w - S_\infty} u$$
$$= \frac{\partial \psi}{\partial Y},$$
$$\cdots \nu = -\frac{\partial \psi}{\partial X} \qquad (6)$$

The notation section defines each parameter. These are introduced into equations (1)-(4) to produce the system non-linear DEs:

$$f''' + ff'' + G_r\theta \sin \alpha - Mf' = 0 \qquad (7)$$
$$\theta'' + \Pr f\theta' + \Pr \bar{\alpha}\theta = 0 \qquad (8)$$
$$\phi'' + P_s f\phi' + P_s S_r\theta'' = 0 \qquad (9)$$

The BCs reduce to:

$$\text{At } f(0) = 0; f'(0) = 0, \theta(0) = \sin \alpha, \phi(0) = 1$$
$$As \quad \eta \to \infty : f' = \theta = \phi = 0 \quad (10)$$

in above differential equations, the η is independent variable and $G_r = 2\,g\beta \left(T_w - T_\infty \right) X/U_0^2$ is Grashof number (thermal), $M = 2\sigma\beta_0^2 X/U_0$ is local MHD body force parameter, $\Pr = \nu\rho C_p/K$ is the Prandtl number, where the modified Prandtl number, $P_s = \nu\rho C_s/K$, the heat source parameter is $\bar{\alpha} = 2XQ^*/U_o\rho C_p$, and the Soret number (thermodiffusion) is $S_r = \frac{F_s}{\nu} \left(\frac{T_w - T_\infty}{S_w - S_\infty} \right)$. Surface shear stress (skin-friction coefficient), Nusselt number (heat transfer rate), and Sherwood number are engineering design parameters that are important for energy systems (salinity transfer rate) which are computed respectively by the following expressions:

$$C_f \left(R_e \right)^{-1/2} = -f''(0) N_u \left(R_e \right)^{-1/2}$$
$$= -\theta'(0) S_h \left(R_e \right)^{-1/2} = -\phi'(0) \qquad (11)$$

where local Reynolds number is denoted by Re.

IV. PROPOSED METHODOLOGICAL APPROACH
Artificial neural networks (ANNs) model the structure and operation of the human brain in a computer. These systems are modelled on the biological cortex, which is dynamic and distributed across hundreds of millions of tiny processors called neurons. ANNs are composed of connected processing components called nodes, which form numerous processing stages called layers that are interconnected into layers at various depths. These form complex processing circuits that recognize patterns in data and produce responses. The patterns can be learned by training to produce layers that associate responses with incoming data in specific patterns knowledge. The network learns through training, and when

connected to other networks, it can learn by sharing information. An ANN's structure is made up of only an input layer, a hidden layer that gets added first and then the output layer. Various industries are using applications of Neural Networks to solve economic, security, and other problems. Neural networks have opened new avenues for research and applications in the data-intensive world. [62], [63]. For data analysis and modelling, AI has recently been extensively used in social science and the arts [64]. Artificial intelligence (AI) has been recently implemented widely to solve optimization problems in various contexts, including business and industrial production and health care. It is one of the new technologies that can benefit from deep learning [64], [65].

The field of artificial intelligence (AI) has advanced to the point where ANNs have proven to be useful models for classification, clustering, pattern recognition, and prediction in various fields. The predictive power of machine learning models is now competitive with that of traditional statistical and regression models [66]. Currently, hotspots and fascinating issues in information and communication technology include AI (machine learning, neural networks, deep learning, robotics), information security, big data, cloud computing, the internet, and forensic science (ICT). In terms of data analysis factors, including accuracy, processing speed, latency, performance, fault tolerance, volume, scalability, and convergence, ANNs' complete applications can be assessed [67], [68]. The high-speed processing offered by ANNs in a massively parallel implementation has considerable potential, which has increased the demand for study in this area [69]. ANNs can be created and used for a variety of tasks, including image recognition and natural language processing. Artificial neural networks (ANNs) are a powerful tool for solving a wide range of problems, including function approximation. They are particularly well-suited for tasks that require the ability to learn and adapt based on experience, as they are able to "learn" from training data and improve their performance over time. ANNs are also highly fault-tolerant, as they can continue functioning even if some of their components fail. Additionally, ANNs can capture non-linear relationships in data, making them useful for modelling complex systems. Finally, ANNs can map input to output with a high degree of accuracy, making them useful for many practical applications [70]. Interconnected neurons and nodes make up the basic building blocks of ANNs. They aggregate input in a specified fashion, accept input, and then perform various nonlinear operations to produce output. The input, weight, threshold, summing junction, and output of an ANN are shown in Figure 2 as their architecture. The connection weights are multiplied by the input t_N in the fundamental model of ANNs, and a bias is added to transform the inputs into the desired outcomes. The net input is computed as follows:

$$u_k = \sum_{k=1}^{N} w_k t_k - \beta_k \qquad (12)$$

To find solution of model i.e outputs $f(\zeta)$, $\theta(\zeta)$ and $\phi(\zeta)$, Log-sigmoid function is taken as activation function, given in equation (13):

$$S(\eta) = \frac{1}{1 + e^{-\eta}}, \qquad (13)$$

where N is the number of inputs. The output (OP) will be become as

$$OP_k = S(u_k) \qquad (14)$$

with more simplified form it will get the shape

$$S(u_k) = \frac{1}{1 + e^{-(w_k t_k - \beta_k)}} \qquad (15)$$

A. TRAINING PROCEDURE OF WEIGHTS

This section discusses the training procedure of weights by using Matlab neural net fitting tool (nf-tool) as a surrogate model. A reference input is required for a surrogate model, which is modelled to the targeted output. The reference input is generated by built-in function of Mathematica NDSolve. The working procedure of NDSolve is based on Runge-Kutta order four (RK4). The reference input or solution is generated between 0 to 1 for 1001 points by taking step size 0.001. For proper validation, training and testing of the problem, Levenberg-Marquardt soft computing technique is used. Furthermore, the solution is evaluated by mean square error (MSE), error histogram, absolute error and regression (R^2).

$$MSE = \frac{1}{k} \sum_{j=1}^{k} \left(x_j(t) - \hat{x}_j(t) \right)^2, \qquad (16)$$

$$R^2 = 1 - \frac{\sum_{j=1}^{k} \left(\hat{x}_j(t) - \bar{x}_j(t) \right)^2}{\sum_{j=1}^{k} \left(x_j(t) - \bar{x}_j(t) \right)^2}, \qquad (17)$$

and

$$AE = \left| x_j(t) - \hat{x}_j(t) \right|, \quad j = 1, 2, \dots, k \qquad (18)$$

V. COMPUTATIONAL EXPERIMENTATION

In order to determine velocity profile, temperature, and salinity profile (f'), θ (ϕ), respectively, variations for the effects of the magneto-hydrodynamic body force parameter (M), the Grashof number (G_r), the Prandtl number (P_r), the modified Prandtl number (P_s), the heat source parameter ($\bar{\alpha}$), and the Soret number (S_r).

In this section, certain examples of the ocean energy generator are considered based on variation of various parameters. The cases of the problem are given in table 1 discussed in this paper.

Example I - Grashof Number: In this example, the vertical plates are considered under the influence of Grashof number (G_r). The inclination of plate depends on angle α. The values of rest of the parameters are given in table 1. By putting values, the model becomes as given:

$$f''' + ff'' + G_r \theta \sin 90° - f' = 0 \qquad (19)$$

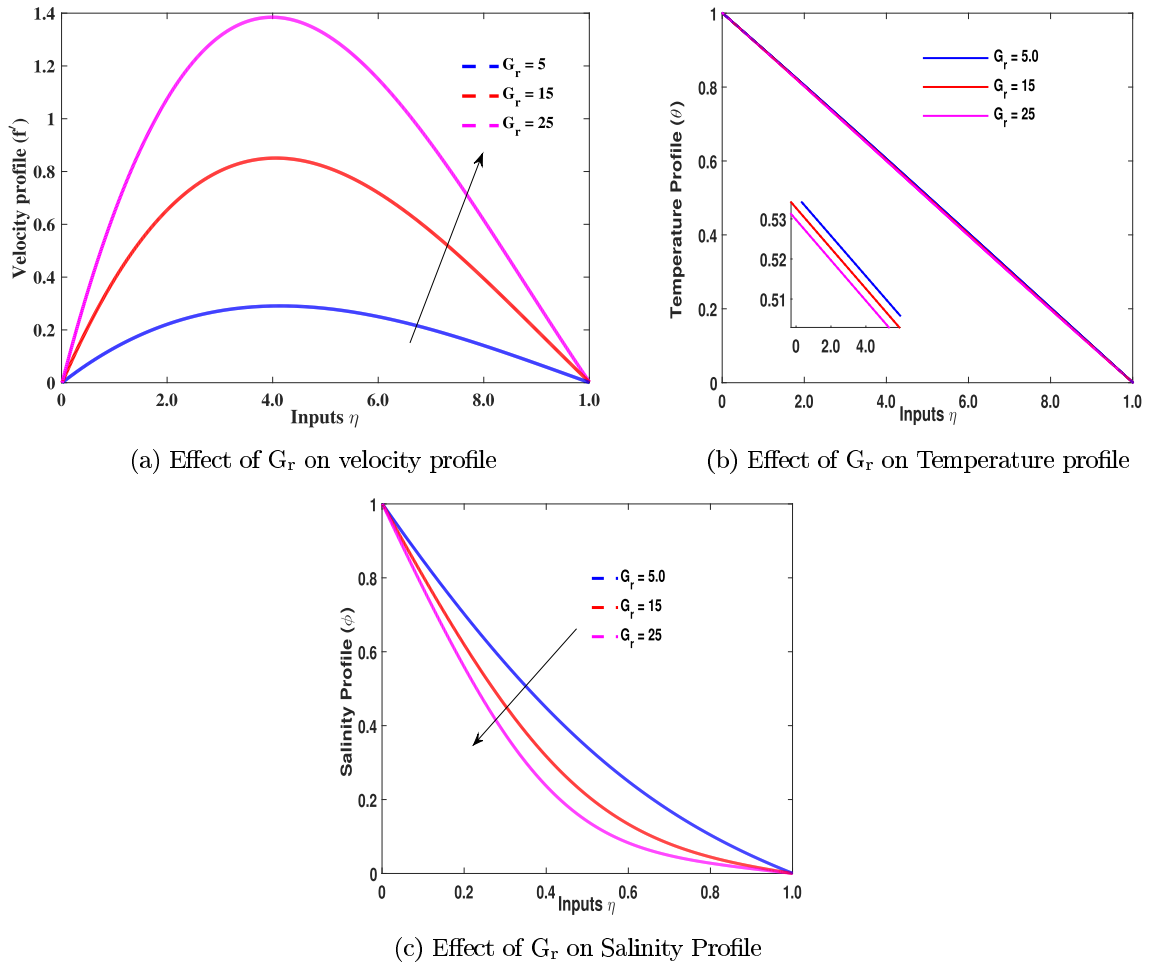$$\theta'' + 0.125 f\theta' + 0.125\theta = 0 \qquad (20)$$

(a) Effect of G_r on velocity profile

(b) Effect of G_r on Temperature profile

(c) Effect of G_r on Salinity Profile

FIGURE 3. Example I: Effect of variations of G_r on velocity, temperature and salinity profile.

TABLE 1. Examples created by variation of parameters.

Example	Case	α	M	$\mathbf{P}_r$	$\bar{\alpha}$	$\mathbf{P}_s$	$\mathbf{S}_r$	$\mathbf{G}_r$
	A	90°	1.0	0.125	1.0	10	1.0	5.0
I	B	90°	1.0	0.125	1.0	10	1.0	15
	C	90°	1.0	0.125	1.0	10	1.0	25
	A	90°	1.0	0.5	0.5	1.0	1.0	4.0
II	B	90°	1.0	0.5	0.7	1.0	1.0	4.0
	C	90°	1.0	0.5	1.0	1.0	1.0	4.0
	A	90°	0.0	0.125	0.5	10	1.0	1.0
III	B	90°	1.0	0.125	0.5	10	1.0	1.0
	C	90°	2.0	0.125	0.5	10	1.0	1.0

$$\phi'' + 10f\phi' + 10\theta'' = 0 \qquad (21)$$

Example II - Heat Source Parameter: In this example the vertical plates are considered under the influence of heat source parameter $\bar{\alpha}$. The inclination of plate depend on angle α. The values of other parameters are given in table 1.

The model is given as:

$$f''' + ff'' + 4\theta \sin 90° - f' = 0 \qquad (22)$$
$$\theta'' + 0.5 f\theta' + 0.5\bar{\alpha}\theta = 0 \qquad (23)$$
$$\phi'' + f\phi' + \theta'' = 0 \qquad (24)$$

Example III - Magnetic Parameter: In this example the vertical plates are considered under the influence of Magnetic parameter M. The inclination of plate depend on angle α. The values of other parameters are given in table 1. The model is given as

$$f''' + ff'' + \theta \sin 90° - Mf' = 0 \qquad (25)$$
$$\theta'' + 0.125 f\theta' + 0.125 \times 0.5\theta = 0 \qquad (26)$$
$$\phi'' + 10f\phi' + 10\theta'' = 0 \qquad (27)$$

A. RESULTS AND DISCUSSION
The network is trained using by taken 10 hidden networks and 15% of data is trained and tested and 75% of data is validated for the evaluation of performance of the network. The performance is also evaluated by regression. The details of each variable and its errors in validation, testing and training

TABLE 2. Training, testing and validation data.

Case	Hidden Neurons	Training	Testing	Validation	Iterations	Regression
A	10	7.52E-12	8.15E-12	9.74E-12	29	1
B	10	3.47E-09	6.53E-09	1.56E-09	57	1
C	10	1.47E-09	3.46E-09	1.56E-09	64	1
A	10	2.41E-09	5.23E-09	1.26E-09	52	1
B	10	9.24E-11	8.31E-11	1.16E-10	21	1
C	10	3.22E-10	5.68E-10	1.18E-10	35	1
A	10	1.95E-11	2.67E-11	2.91E-11	124	1
B	10	7.00E-12	8.22E-12	8.16E-12	103	1
C	10	1.09E-09	1.21E-09	1.17E-09	125	1

TABLE 3. Training, testing and validation data.

Problem	Case	Hidden Neurons	Training	Testing	Validation	Iterations	Regression
I	A	10	7.65E-15	6.28E-15	6.28E-15	129	1.0
	B	10	1.12E-15	4.57E-15	5.04E-15	128	1.0
	C	10	2.20E-14	8.88E-15	1.18E-15	123	1.0
II	A	10	2.35E-15	6.22E-15	4.81E-15	123	1.0
	B	10	1.95E-13	3.10E-13	2.89E-13	127	1.0
	C	10	8.85E-15	8.88E-15	9.81E-15	128	1.0
III	A	10	2.20E-14	2.08E-14	2.56E-14	141	1.0
	B	10	4.80E-15	4.40E-15	4.61E-15	128	1.0
	C	10	4.89E-15	4.92E-15	5.03E-15	128	1.0

TABLE 4. Example I: Numerical comparison of proposed results and RK4.

	$G_r = 5.0$						$G_r = 15$						$G_r = 25$					
η	$f'(\eta)$		$\theta(\eta)$		$\phi(\eta)$		$f'(\eta)$		$\theta(\eta)$		$\phi(\eta)$		$f'(\eta)$		$\theta(\eta)$		$\phi(\eta)$	
	Proposed	RK4	Proposed	RK4	Proposed	RK4	Proposed	RK4	Proposed	RK4	Proposed	RK4	Proposed	RK4	Proposed	RK4	Proposed	RK4
0.0	0.0000000	0.0000000	1.0000000	1.0000000	1.0000000	1.0000000	0.0000000	0.0000000	1.0000000	1.0000000	1.0000000	1.0000000	0.0000000	0.0000000	1.0000000	1.0000000	1.0000000	1.0000000
0.25	0.2521457	0.2521459	0.7559243	0.7559242	0.6198106	0.6198106	0.7445232	0.7445231	0.7540120	0.7540120	0.5211940	0.5211940	1.2215996	1.2215997	0.7521808	0.7521807	0.4519714	0.4519714
0.50	0.2820272	0.2820271	0.5062552	0.5062551	0.3269603	0.3269604	0.8190221	0.8190222	0.5030546	0.5030547	0.2000098	0.2000098	1.3220837	1.3220839	0.5000053	0.5000052	0.1338106	0.1338105
0.75	0.1723245	0.1723245	0.2534709	0.2534710	0.1278976	0.1278975	0.4862981	0.4862980	0.2506345	0.2506345	0.0565351	0.0565352	0.7636830	0.7636830	0.2479562	0.2479563	0.0348123	0.0348125
1.0	0.0000000	0.0000000	0.0000000	0.0000000	0.0000000	0.0000000	0.0000000	0.0000000	0.0000000	0.0000000	0.0000000	0.0000000	0.0000000	0.0000000	0.0000000	0.0000000	0.0000000	0.0000000

TABLE 5. Example II: Numerical comparison of proposed results and RK4.

	$\bar{\alpha} = 0.5$						$\bar{\alpha} = 0.7$						$\bar{\alpha} = 1.0$					
η	$f'(\eta)$		$\theta(\eta)$		$\phi(\eta)$		$f'(\eta)$		$\theta(\eta)$		$\phi(\eta)$		$f'(\eta)$		$\theta(\eta)$		$\phi(\eta)$	
	Proposed	RK4	Proposed	RK4	Proposed	RK4	Proposed	RK4	Proposed	RK4	Proposed	RK4	Proposed	RK4	Proposed	RK4	Proposed	RK4
0.0	0.0000000	0.0000000	1.0000000	1.0000000	1.0000000	1.0000000	0.0000000	0.0000000	1.0000000	1.0000000	1.0000000	1.0000000	0.0000000	0.0000000	1.0000000	1.0000000	1.0000000	1.0000000
0.25	0.1476724	0.1476725	0.6481338	0.6481337	0.7356224	0.7356224	0.2050854	0.2050855	0.7664112	0.7664112	0.7273943	0.7273942	0.2078807	0.2078806	0.7751357	0.7751357	0.7186309	0.7186314
0.50	0.1659066	0.1659067	0.4357642	0.4357643	0.4822367	0.4822369	0.2302525	0.2302526	0.5170789	0.5170789	0.4726231	0.4726232	0.2339626	0.2339627	0.5271026	0.5271026	0.4625747	0.4625746
0.75	0.1020186	0.1020186	0.2182782	0.2182781	0.2378369	0.2378369	0.1411989	0.1411988	0.2592167	0.2592167	0.2317154	0.2317152	0.1436697	0.1436698	0.2654598	0.2654598	0.2254913	0.2254913
1.0	0.0000000	0.0000000	0.0000000	0.0000000	0.0000000	0.0000000	0.0000000	0.0000000	0.0000000	0.0000000	0.0000000	0.0000000	0.0000000	0.0000000	0.0000000	0.0000000	0.0000000	0.0000000

is given in table 2 and 3. While the comparison of results are reported in table 4 and 5.

In figure 3, the velocity, temperature and salinity profiles of Example I are given. The effect in these profiles is due to variation in Grashof number (G_r). In figure 3a, the velocity profile increases and, by achieving its maximum value, decreases. The behaviour of velocity profile gives the parabolic shape. While the variation of G_r do not much effect the temperature profile. And the salinity profile can observe in figure 3c with increase in G_r value.

As in figure 3, for some distance from the plate surface into the boundary layer, a large decrease in velocity coincides with a rise in Grashof number. $G_r = 2 \, g\beta \left(T_w - T_\infty\right) X/U_0^2$. The parameter replicates the relationship between the buoyancy (natural convection) and the viscosity in the region. Viscous

force is outweighed by buoyant force when $G_r > 1$. As a result, the flow slows down closer to the plate surface as buoyancy increases. The magnitudes of the velocity decrease with increasing inclination angle as opposed to $\alpha = 90°$. It is obvious that the no change in G_r will decrease the buoyancy force as $sin 90 (= 1) > sin 120 (= 0.8660)$. The buoyancy force over vertical plate will be greater than the buoyancy force over inclined plate, which will slow down the former. Therefore, plate orientation is a crucial geometric factor that can be used to alter the MHD ocean generating system's transport properties.

The performance of NN-LMA on example I is given in figure 4. These data out of 100%, 15% is tested, 15% is validated, and the rest of 70% is trained. From figures, it can observe that the training, testing and validation converge
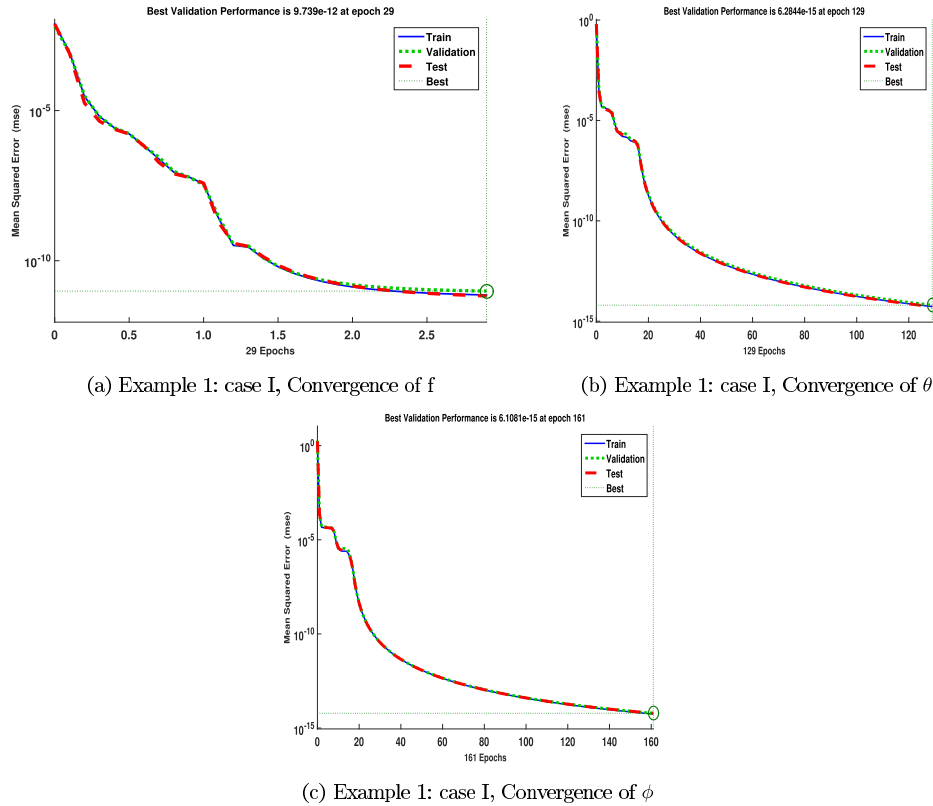
(a) Example 1: case I, Convergence of f

(b) Example 1: case I, Convergence of θ

(c) Example 1: case I, Convergence of φ

FIGURE 4. Example I: Convergence graphs.

(a) Effect of ᾱ and P_s on velocity profile

(b) Effect of ᾱ and P_s on Temperature profile
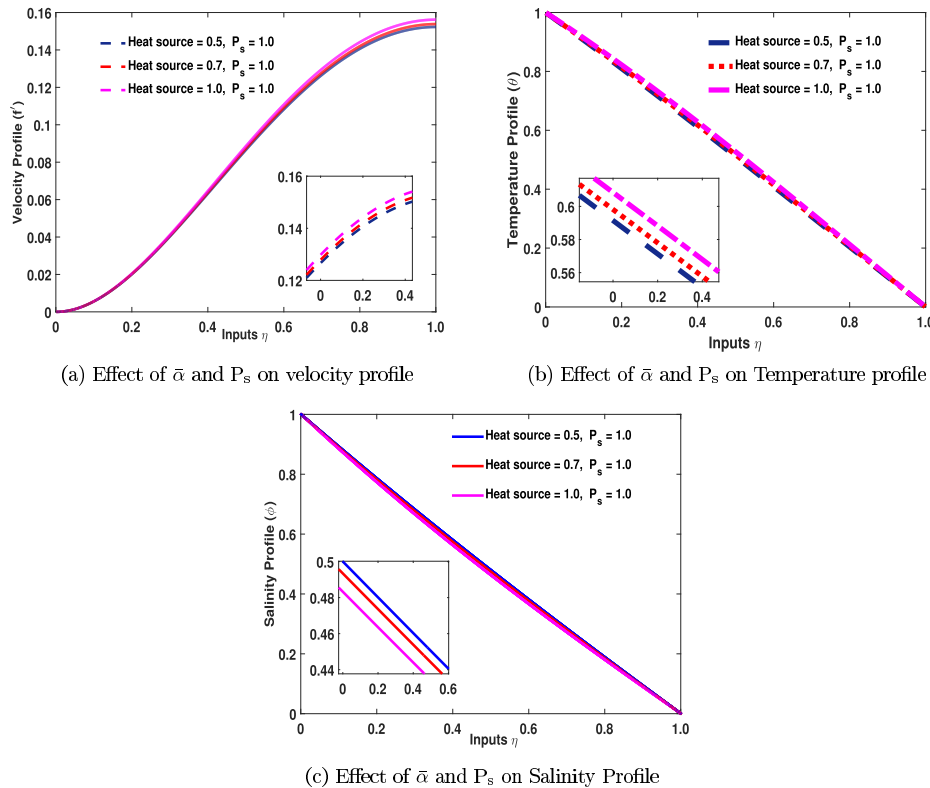

(c) Effect of ᾱ and P_s on Salinity Profile

FIGURE 5. Example II: Effect of variations of $\bar{\alpha}$ and P_S on velocity, temperature and salinity profile.

to the same point, which shows the best performance of NN-LMA. The performance is evaluated by mean square error (MSE). In figure 4a, b and c, the performance/MSE lies in between 10^{-12}-10^{-15}.

(a) Example II: Convergence graphs of f

(b) Example II: Convergence graphs of θ

(c) Example II: Convergence graphs of ϕ
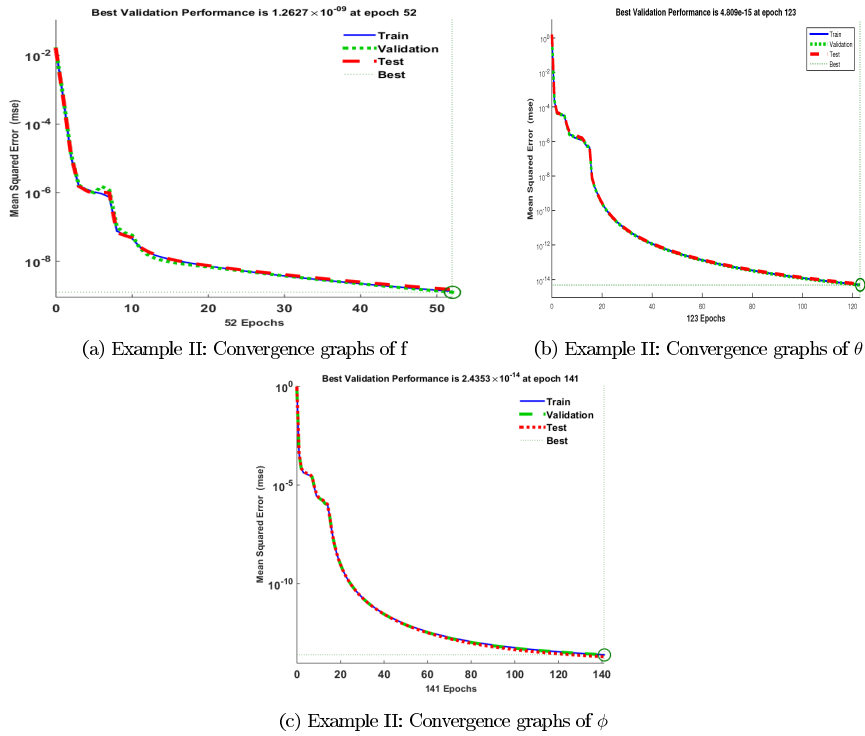
FIGURE 6. Example II: Case-A convergence graphs.

(a) Performance graph of f

(b) Performance graph of θ

(c) Performance graph of ϕ
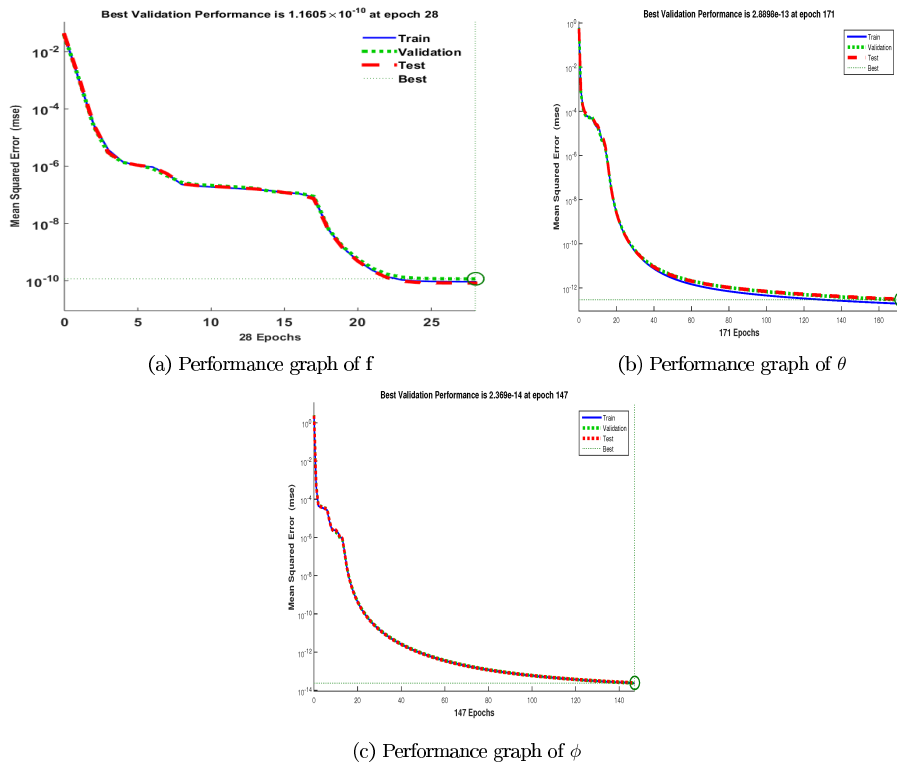
FIGURE 7. Example II: Case-B performance graph.

The velocity, temperature and salinity profiles of example II are given in figure 5. A slight velocity increase is observed with parameter $\bar{\alpha}$ and Ps at an inclination of 90°. The velocity, temperature and salinity profiles are shown in subfigure 5a, b and c, respectively.

In figure 6-8, the performance of example II is given each sub-figure a, b and c shows the performance of variable f, θ and ϕ. The performance of Case-A is given in figure 6. The training, testing and validation converge to same point. The best performance value of Case-A is between $10^{-09} - 10^{-15}$,

(a) Performance graph of f

(b) Performance graph of θ

(c) Performance graph of η
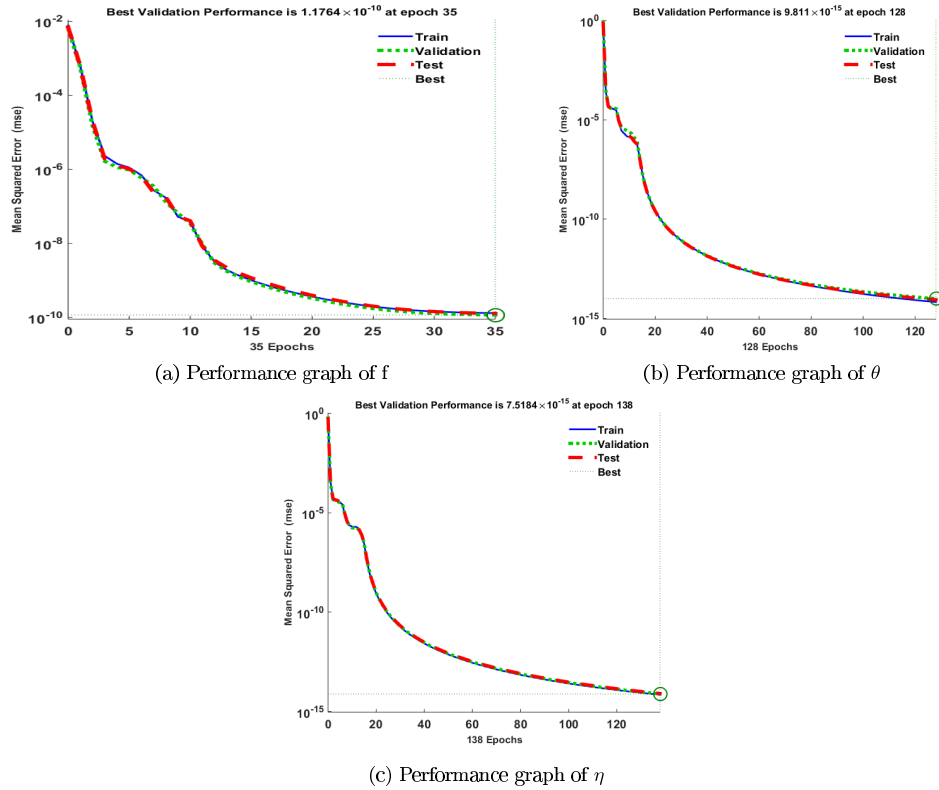
FIGURE 8. Example II: Case-C performance graphs.

(a) Effect of magnetic parameter on velocity profile

(b) Effect of magnetic parameter on Temperature profile

(c) Effect of magnetic parameter on Salinity Profile
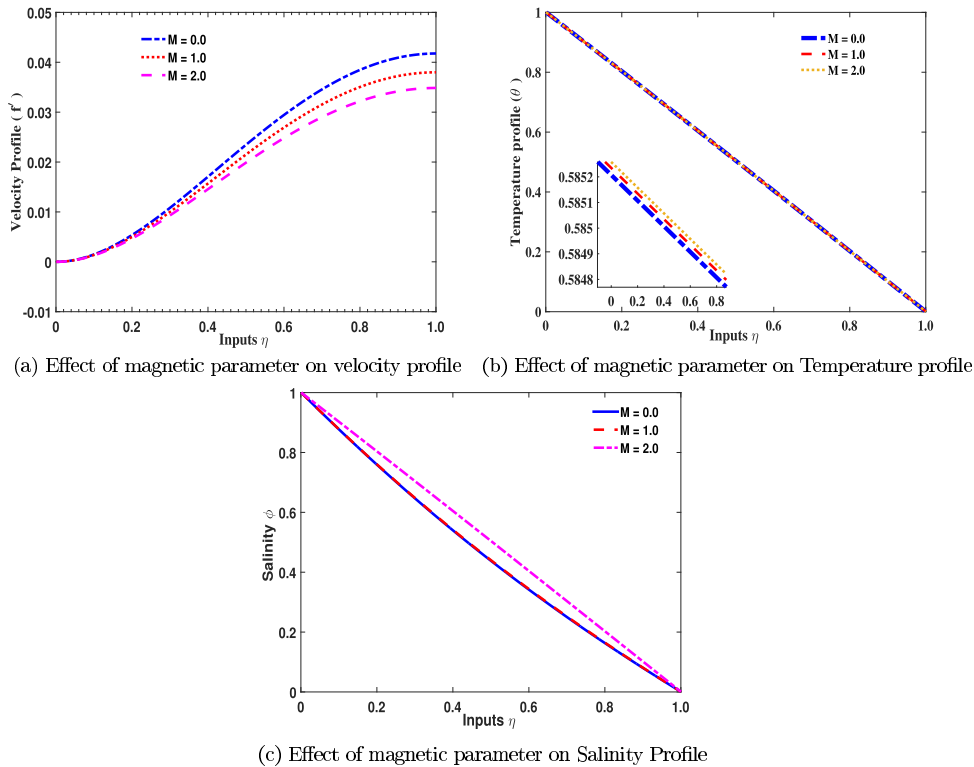
FIGURE 9. Example III: Effect of variations of magnetic parameter on velocity, temperature and salinity profile.

the values of Case-B is between $10^{-10} - 10^{-14}$ and the performance values of Case-C lies between $10^{-10} - 10^{-15}$.

The velocity, temperature and salinity profiles of example II are given in figure 9. The performance of Example III is

(a) Performance graph of f

(b) Performance graph of θ

(c) Performance graph of ϕ
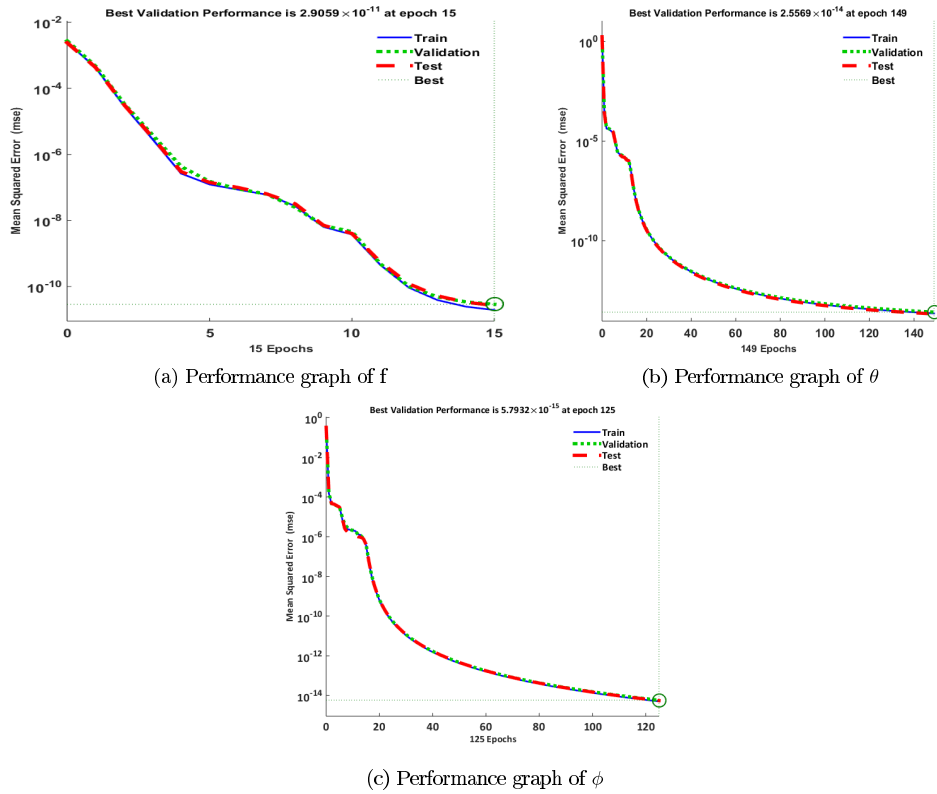
FIGURE 10. Example III: Case-A performance graphs.

(a) Performance graph of f

(b) Performance graph of θ

(c) Performance graph of ϕ
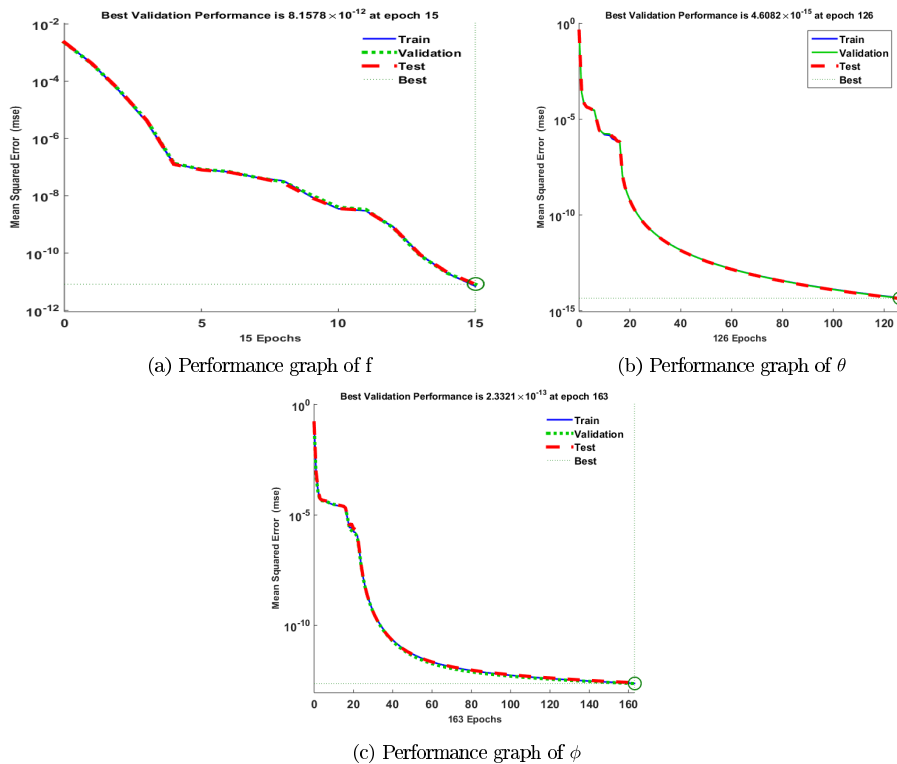
FIGURE 11. Example III: Case-B performance graphs.

given in figures 10-12. The data of training, validation and testing converges to the same point. Which shows the best performance of the NN-LMA technique. The MSE of Case-A for each variable is between $10^{-11} - 10^{-15}$, the value for Case-B lies between $10^{-12} - 10^{-15}$ and for Case-C MSE are $10^{-09} - 10^{-15}$.

(a) Performance graph of f

(b) Performance graph of θ

(c) Performance graph of φ
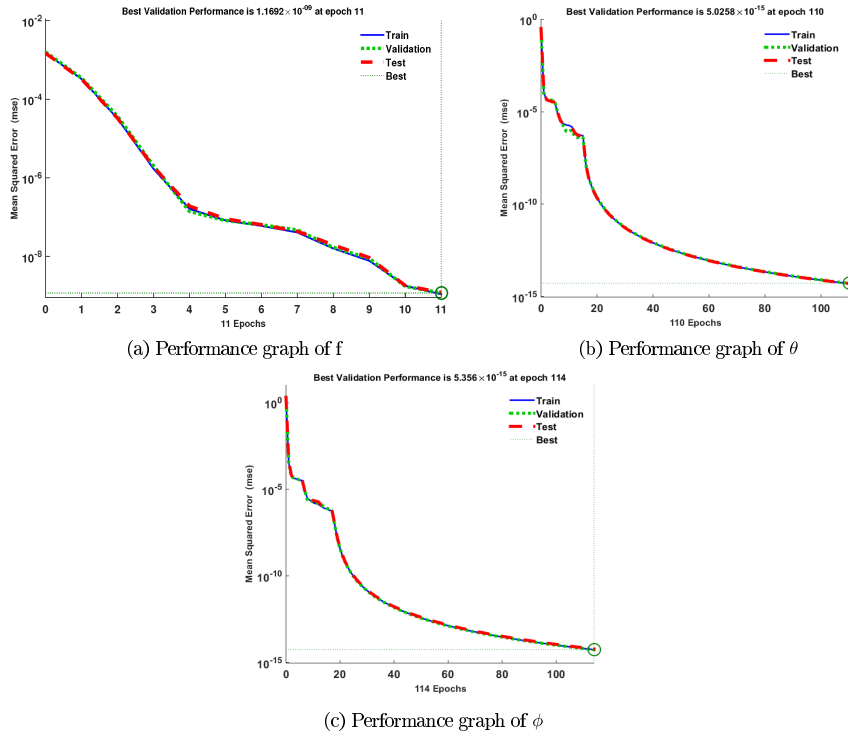
FIGURE 12. **Example III: Case-C performance graphs.**

(a) Analysis of solution via regression f

(b) Analysis of solution via regression θ

(c) Analysis of solution via regression φ
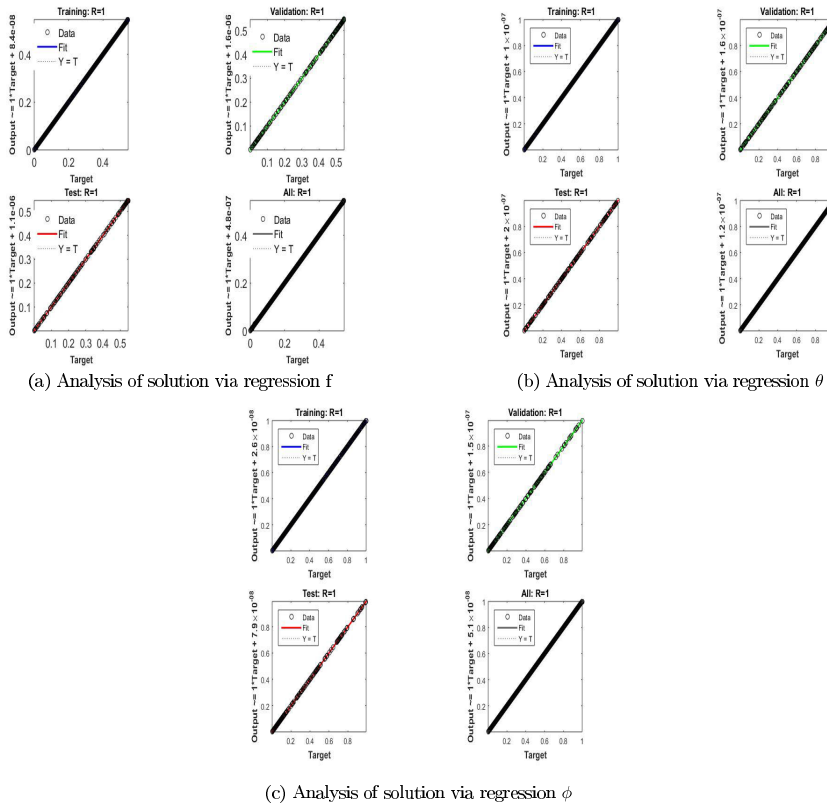
FIGURE 13. **Example I: Analysis of solution via regression obtain by NN-LMA.**

B. EVALUATION OF NN-LMA BY REGRESSION

Regression is used to determine the strength of the data. As much the regression value converges to 1; it indicates better data. The data of validity, training, and testing is also evaluated by regression. Each data that is validation training and testing is evaluated separately, and this data is combined

(a) Analysis of solution via regression f

(b) Analysis of solution via regression θ

(c) Analysis of solution via regression ϕ
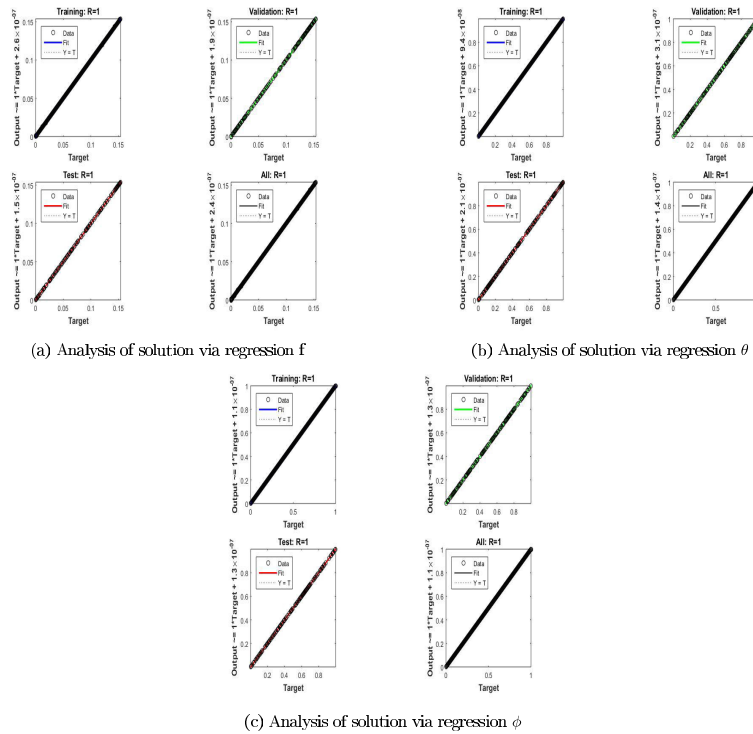
FIGURE 14. Example II: Case-B analysis of solution via regression obtain by NN-LMA.

(a) Analysis of solution via regression f

(b) Analysis of solution via regression θ

(c) Analysis of solution via regression ϕ
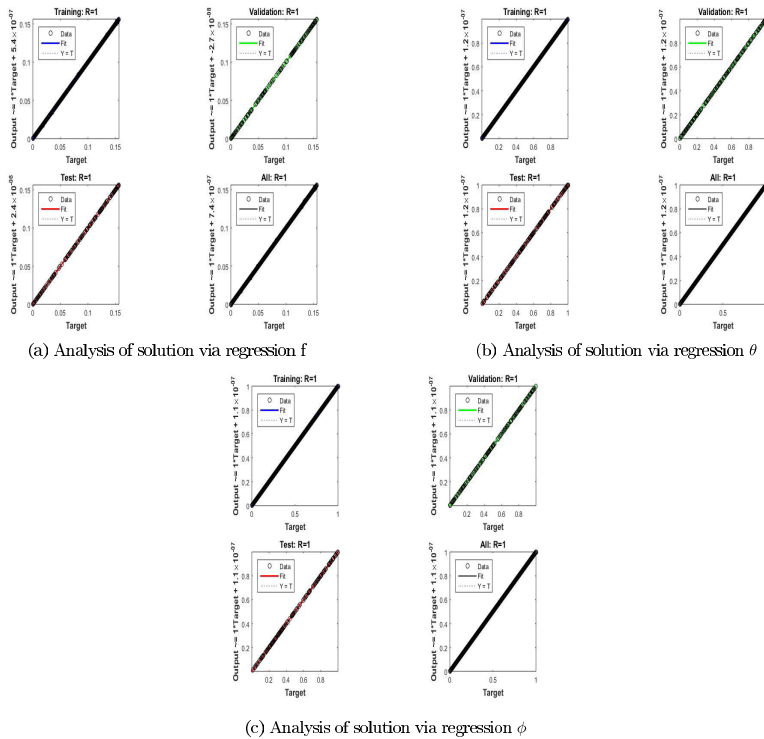
FIGURE 15. Example II: Case-C analysis of solution via regression obtain by NN-LMA.

and analyzed. The analysis is given in the figures 13-18. In figures, 13-18, in each subfigure, first, second and third figure shows a regression for training, validation and testing, respectively. While the fourth figure shows regression of whole data.

The regression figure, for example I is given in figure 13. In each case, it can be seen that the regression is 1, which indicates the best performance of proposed procedure. Along y-axis, the given expression is the surrogate solution, for example I. In figure 14-15, the regression of example II
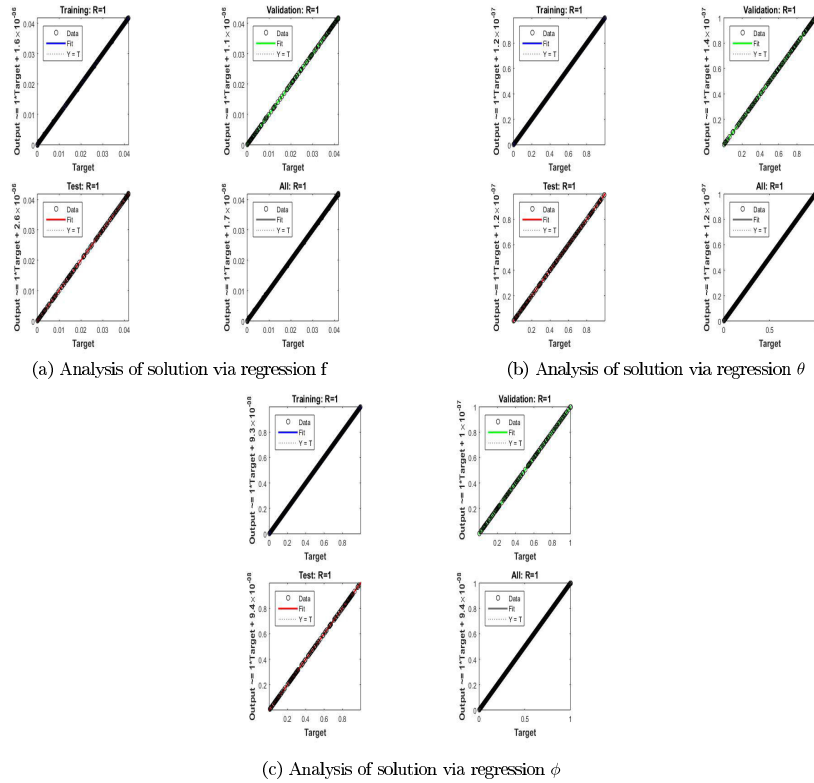
(a) Analysis of solution via regression f

(b) Analysis of solution via regression θ

(c) Analysis of solution via regression φ

FIGURE 16. Example III: Case-A analysis of solution via regression obtain by NN-LMA.

(a) Analysis of solution via regression f

(b) Analysis of solution via regression θ

(c) Analysis of solution via regression φ
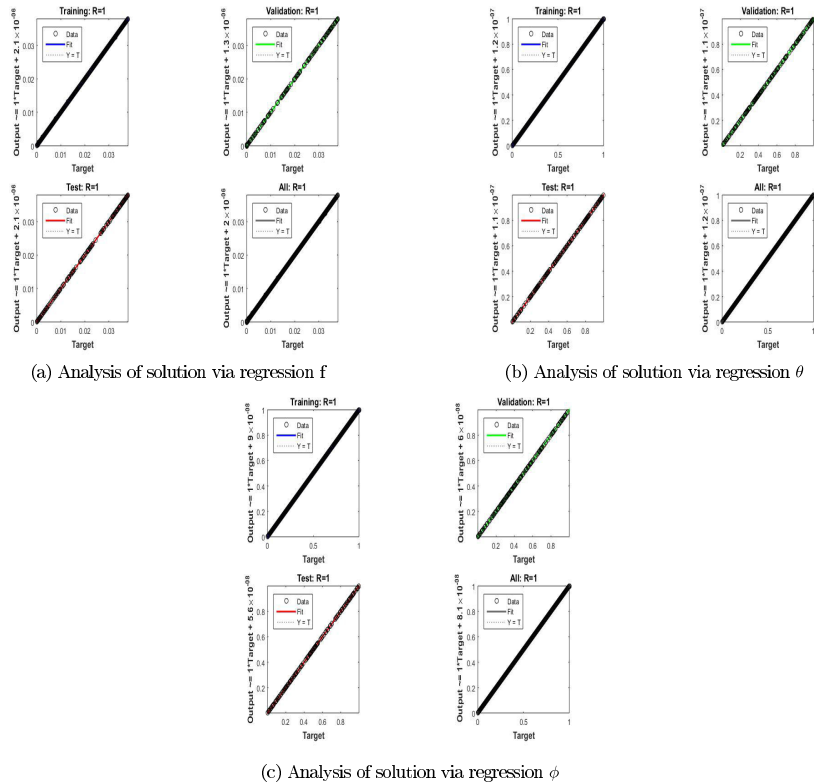
FIGURE 17. Example III: Case-B analysis of solution via regression obtain by NN-LMA.

is given. The two cases of example II are presented. The regression in both cases is 1. The data of example II is also split in training, validation and testing. The surrogate solution is also given along y-axis for each case. The figures 16-18

(a) Analysis of solution via regression f

(b) Analysis of solution via regression θ

(c) Analysis of solution via regression ϕ
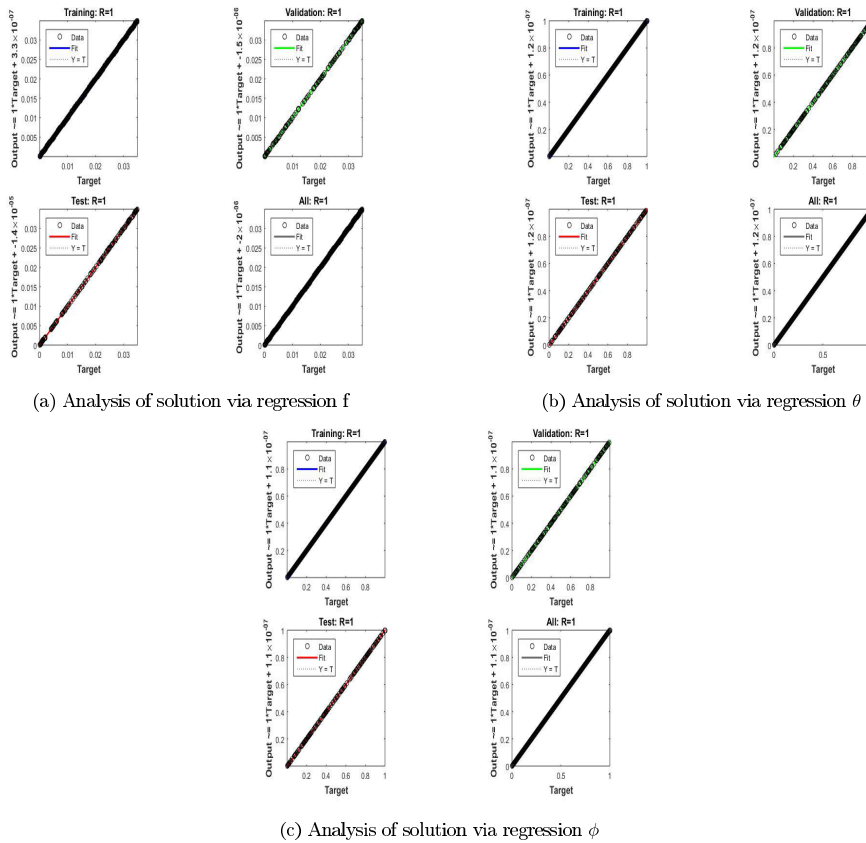
FIGURE 18. Example III: Case-C analysis of solution via regression obtain by NN-LMA.

(a) Training Statistic of f
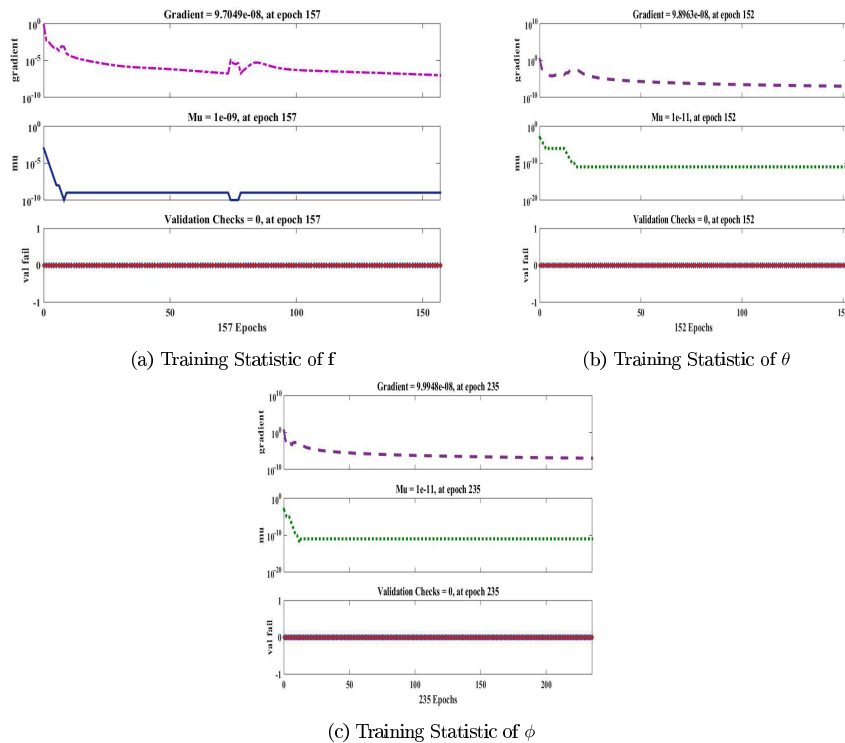
(b) Training Statistic of θ

(c) Training Statistic of ϕ

FIGURE 19. Example I: Case-A training statistics.

are regression of performance of example III. All three cases are given. Similarly, as in example I and example II, the data of example III is also distributed in training, validation and testing.

(a) Training Statistic of f

(b) Training Statistic of θ

(c) Effect of dynamic wedge on $f'(\eta)$
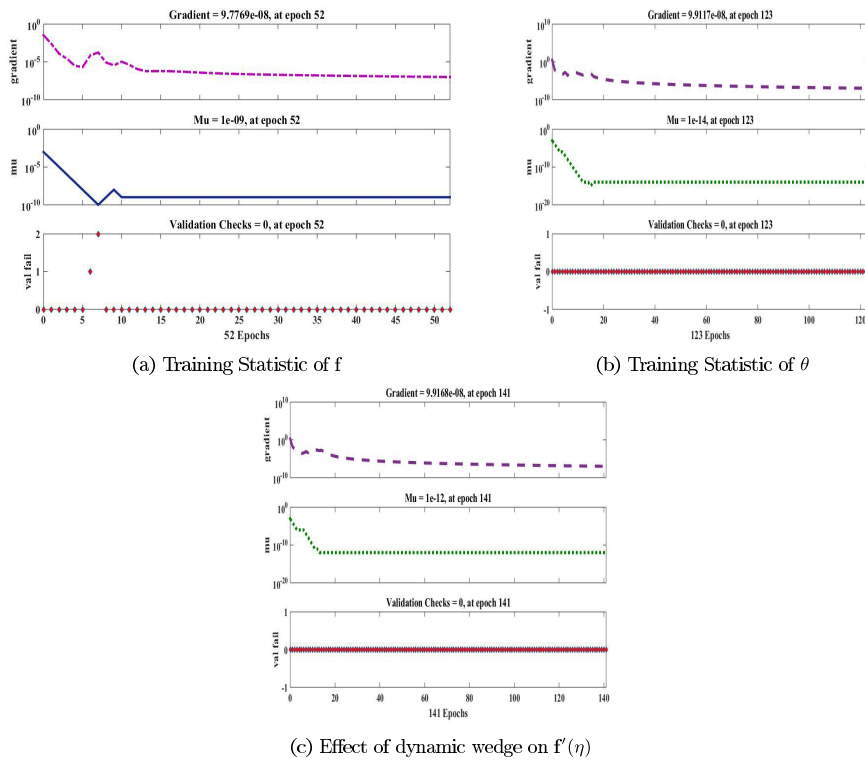
FIGURE 20. Example II: Case-A training statistics.

(a) Training Statistic of f

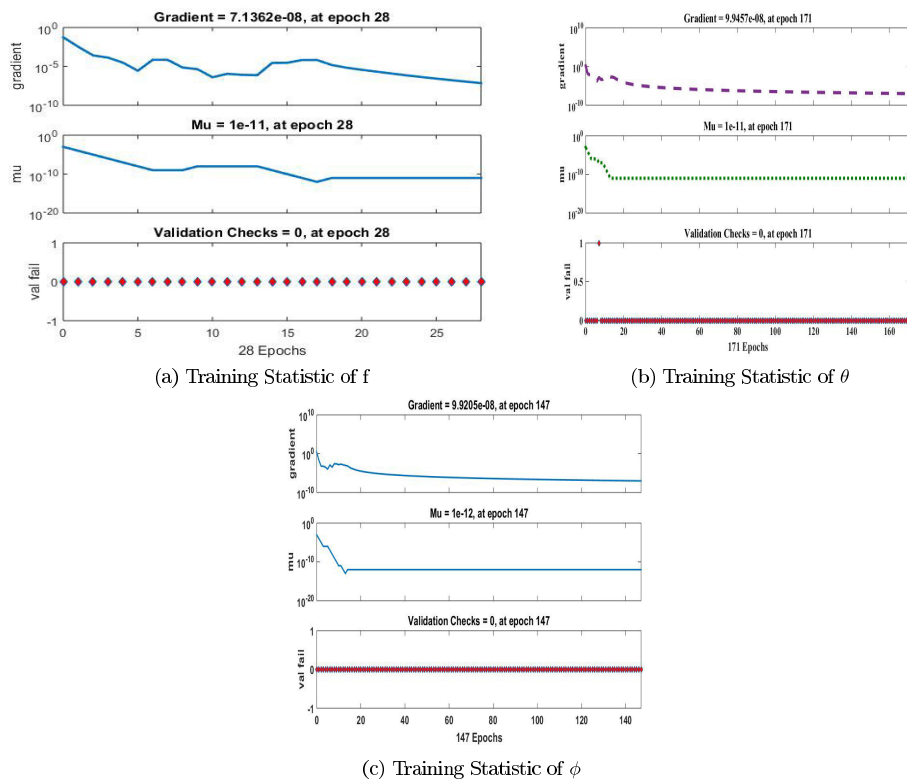(b) Training Statistic of θ

(c) Training Statistic of ϕ

FIGURE 21. Example II: Case-B training statistics.

C. TRAINING STATISTICS

This section is about the provision of statistic of solutions. The statistics of each solution obtained by NN-LMA are given in figures 19-24. The minimum mean square error, validation check and number of iterations are shown in figures.

(a) Training Statistic of f

(b) Training Statistic of θ

(c) Training Statistic of ϕ
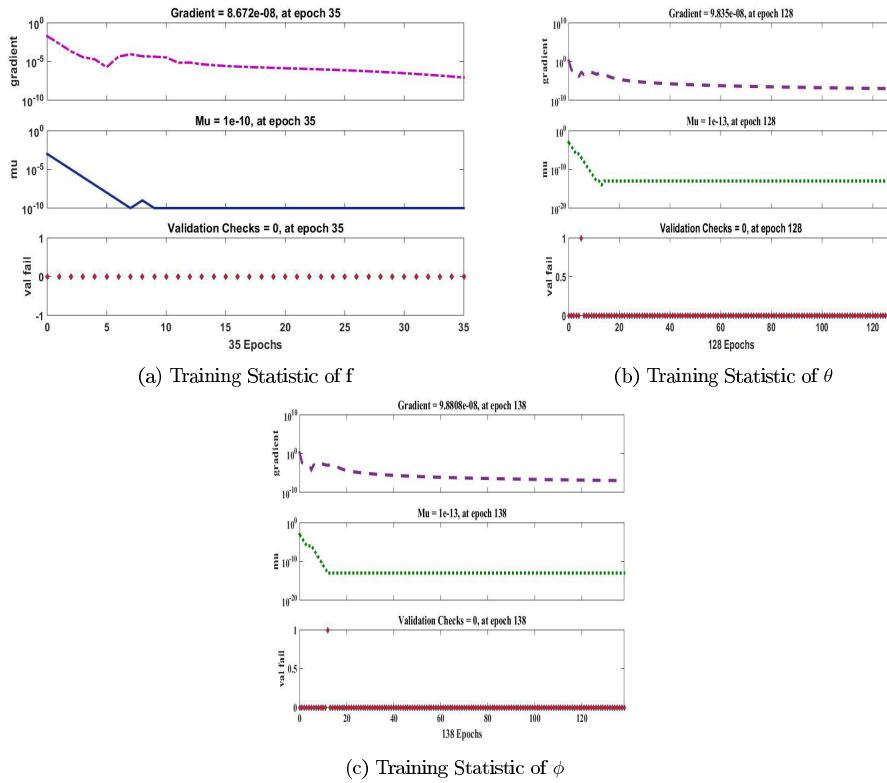
FIGURE 22. Example II: Case-C training statistics.

(a) Training Statistic of f

(b) Training Statistic of θ
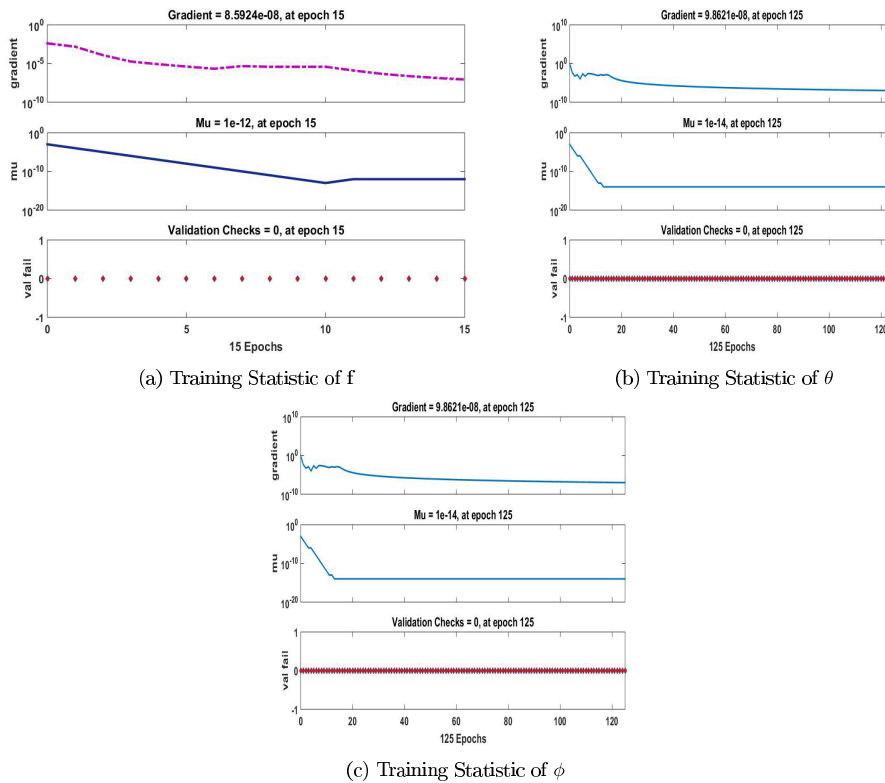
(c) Training Statistic of ϕ

FIGURE 23. Example III: Case-A training statistics.

The statistic of example I is given in figure 19. The gradient of each variable lies about 10^{-08} with iteration from 152 to 235. The validation check for all the variable f, θ and ϕ are zero and Mu lies between
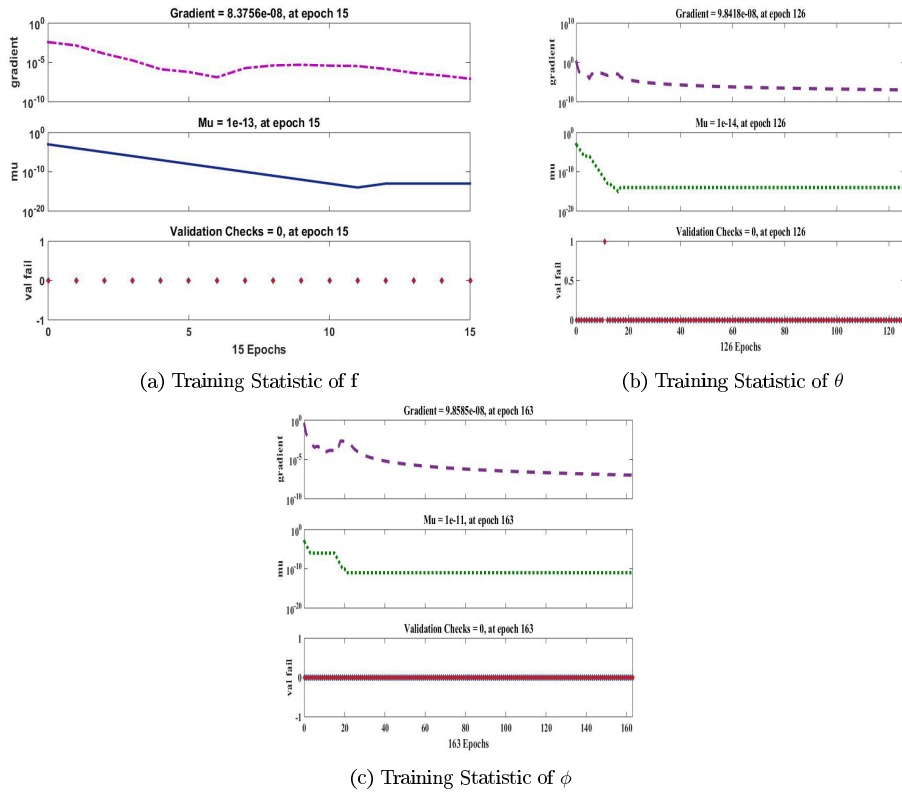
(a) Training Statistic of f

(b) Training Statistic of θ

(c) Training Statistic of ϕ

FIGURE 24. Example III: Case-B training statistics.

(a) Error histogram of f

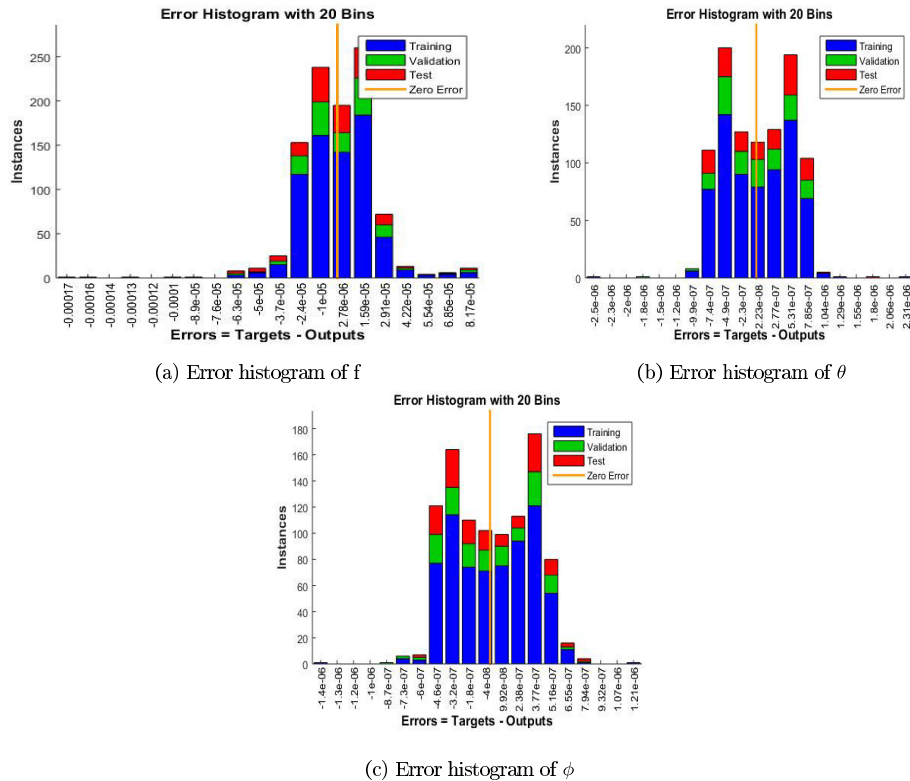(b) Error histogram of θ

(c) Error histogram of ϕ

FIGURE 25. Example I: Case-B error graphs.

10^{-09} - 10^{-11}. The statistics of example II are given in figure 20-22. The gradient of each variable lies about

$10^{-08} - 10^{-09}$. The solution of case-A is obtain by iteration from 52 to 141. The validation check for all the variable f,
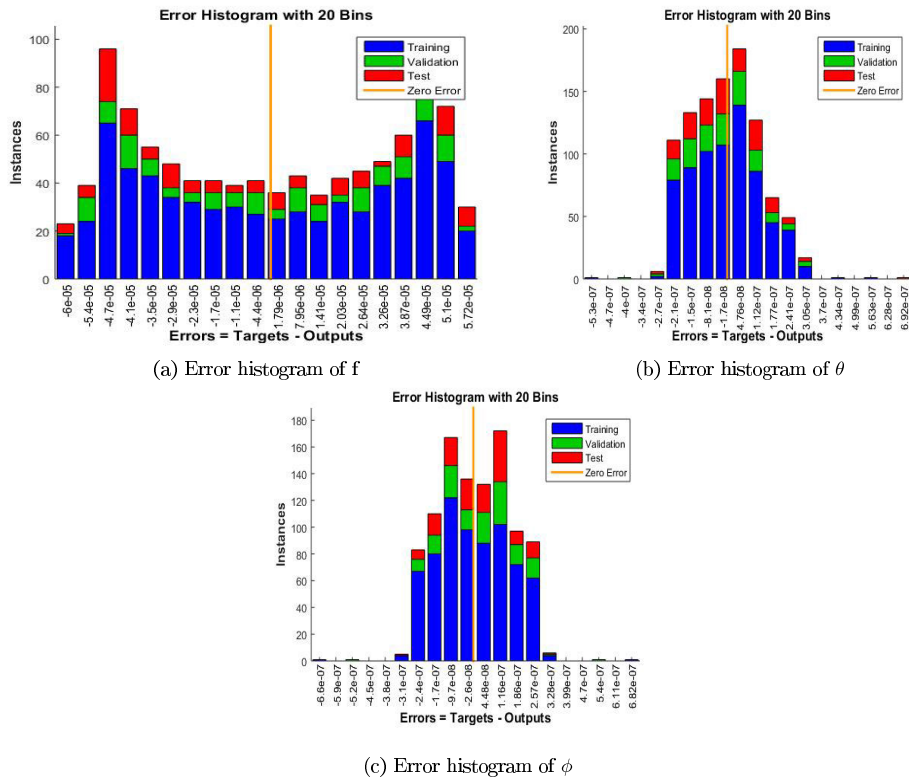
(a) Error histogram of f

(b) Error histogram of θ

(c) Error histogram of ϕ

FIGURE 26. Example II: Case-A error graphs.

(a) Error histogram of f

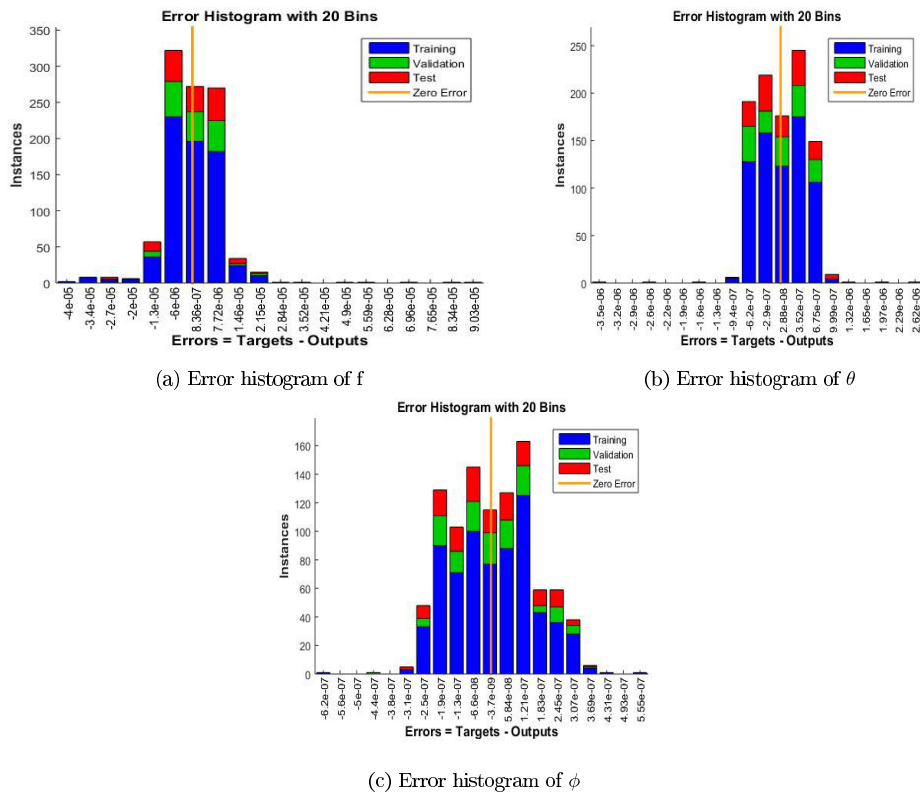(b) Error histogram of θ

(c) Error histogram of ϕ

FIGURE 27. Example II: Case-B error graphs.

θ and ϕ are zero and Mu lies between 10^{-09} - 10^{-12}. For case-B, the iteration are 28-171 and Mu lies between

10^{-09} - 10^{-12}. For case-C, the iteration are 35-138 and Mu lies between 10^{-10} - 10^{-13}. The statistics of example III

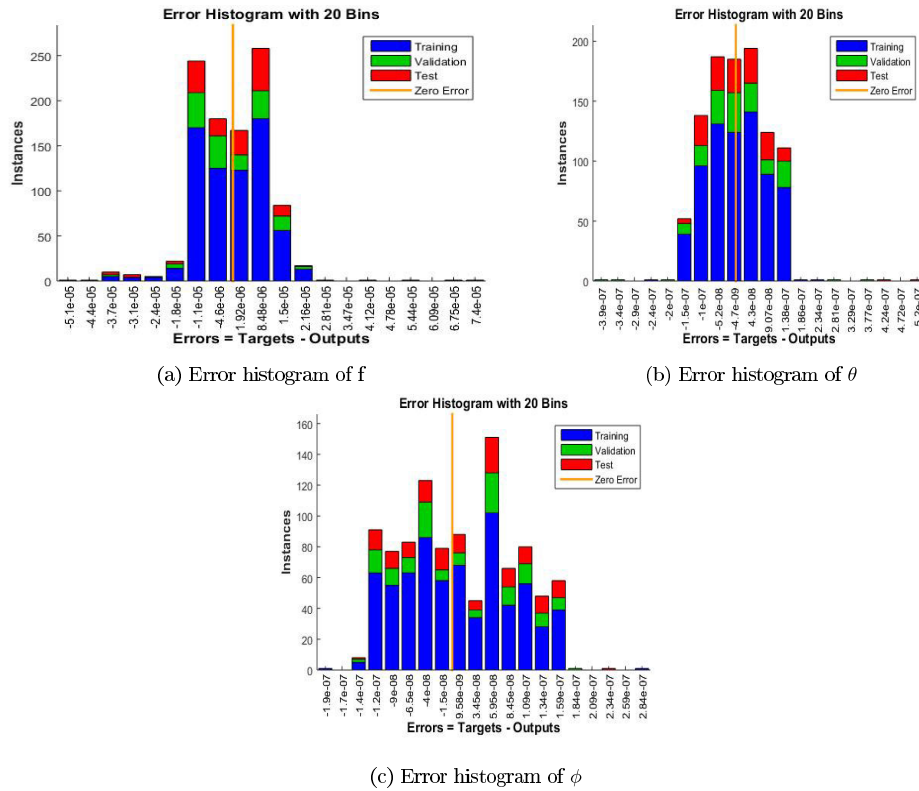(a) Error histogram of f

(b) Error histogram of θ

(c) Error histogram of ϕ

FIGURE 28. Example II: Case-C error graphs.

(a) Error histogram of f

(b) Error histogram of θ
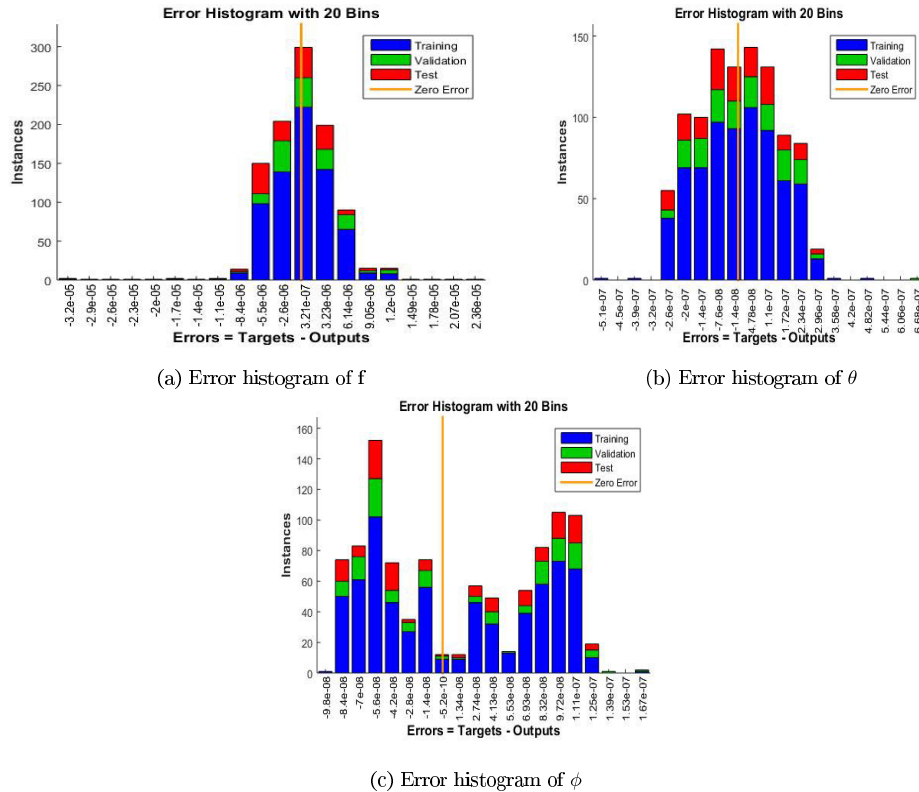

(c) Error histogram of ϕ

FIGURE 29. Example III: Case-A error graphs.

are given in figure 23-24. The gradient of each variable lies about 10^{-08}. The solution of case-A is obtain by iteration from 15 to 125. The validation check for all the variable f, θ and ϕ are zero and Mu lies between 10^{-12} - 10^{-14}.
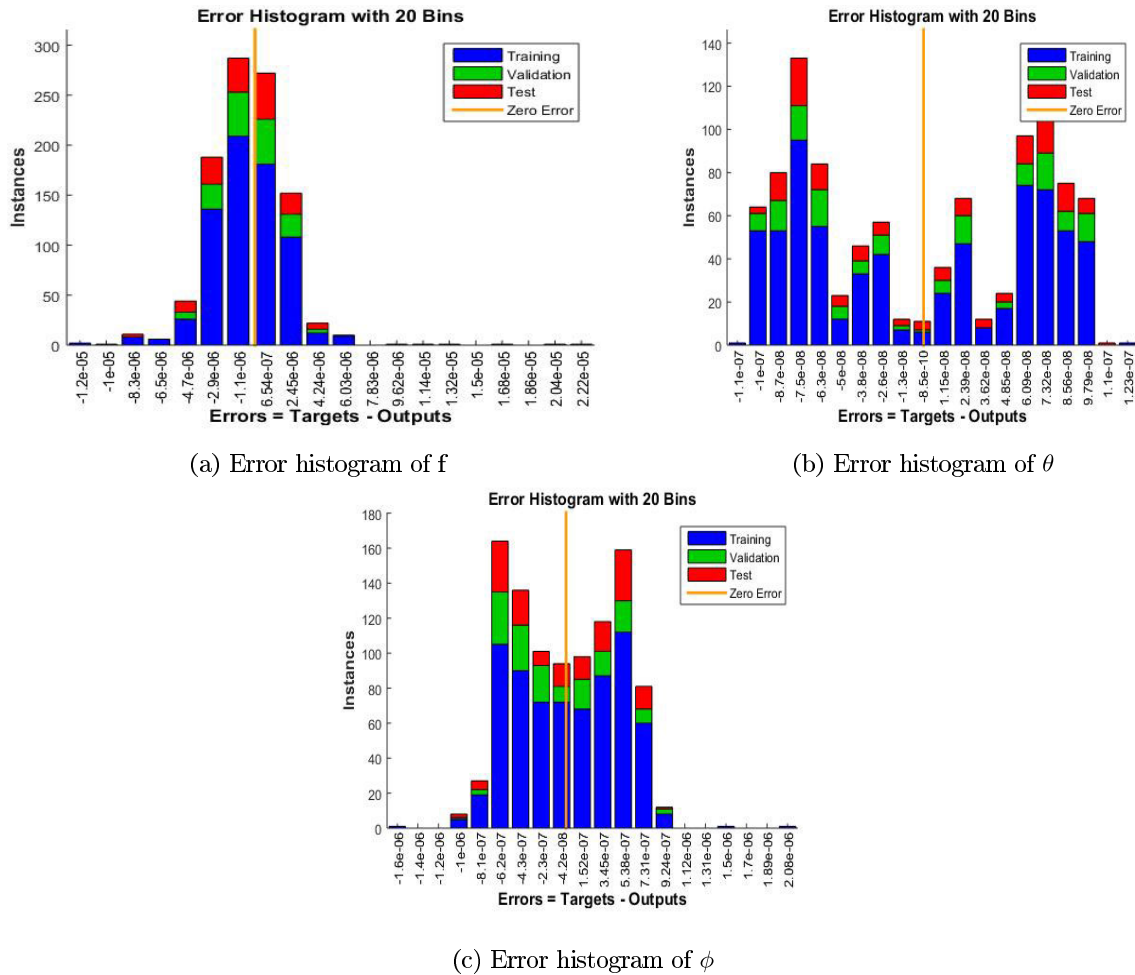
(a) Error histogram of f

(b) Error histogram of θ

(c) Error histogram of ϕ

FIGURE 30. Example III: Case-B error graphs.

For case-B, the iteration are 15-163 and Mu lies between 10^{-11} - 10^{-14}.

D. ERROR HISTOGRAM
An error histogram represents the distribution of errors in a dataset or model predictions. It provides a visual representation of the frequency or count of different error values. The numerical meaning of an error histogram can vary depending on the context, but it typically indicates the distribution of errors, allowing to analyze the bias, variability, or overall performance of a model. The error in training, validation and training data is drawn using histogram. The drawn histograms are given in figures 25-31. The histograms for all the examples are distributed in 20 Bins. The midline shows zero error. The left side of zero error consists of errors from minimum to maximum error, and negative side also shows errors from minimum to maximum.

The histogram of example I case-B is given in figure 25. The errors in each variable are given in separate figures. From figure, it can be seen that all the errors are accumulated about zero error. The error in f is about 10^{-5} and 10^{-7}, in θ errors lies in the range $10^{-7} - 10^{-8}$ and similarly, the errors in ϕ are also about $10^{-7} - 10^{-8}$.

Based on the analysis of ranges of errors, the error histograms in all figures shows that the errors are centered around zero. This indicates, the model's predictions are close to the true values.

The histograms of example II are presented in figures 26-28. In figure 26, the histogram of case-A can be observed. The errors in f are spread over all 20 bins and lie in a range $10^{-5} - 10^{-6}$. The errors in θ and ϕ are converged toward zero errors and lies between $10^{-7} - 10^{-8}$.

In figure 27, the histograms of case-B are reported. The errors in f lies in a range $10^{-5} - 10^{-7}$. The errors in θ and ϕ are lies between $10^{-7} - 10^{-8}$ and the range of ϕ is $10^{-7} - 10^{-9}$. All the errors are accumulated about zero errors. The histogram of case-C is given in figure 28. All variables' errors are in the range $10^{-5} - 10^{-8}$. The histograms of example II are presented in figures 29-31. In figure 29, the histogram of case-A can be observed. The errors in f are lies in a range $10^{-6} - 10^{-7}$. The errors in θ and ϕ are converged toward zero errors and lies between $10^{-7} - 10^{-10}$.

Figure 30 presents the histograms of case-B. The errors in f lies in a range $10^{-6} - 10^{-7}$. The errors in θ and ϕ are lies between $10^{-7} - 10^{-10}$ and the range of ϕ is $10^{-7} - 10^{-8}$. All the errors are accumulated about zero errors. The histogram
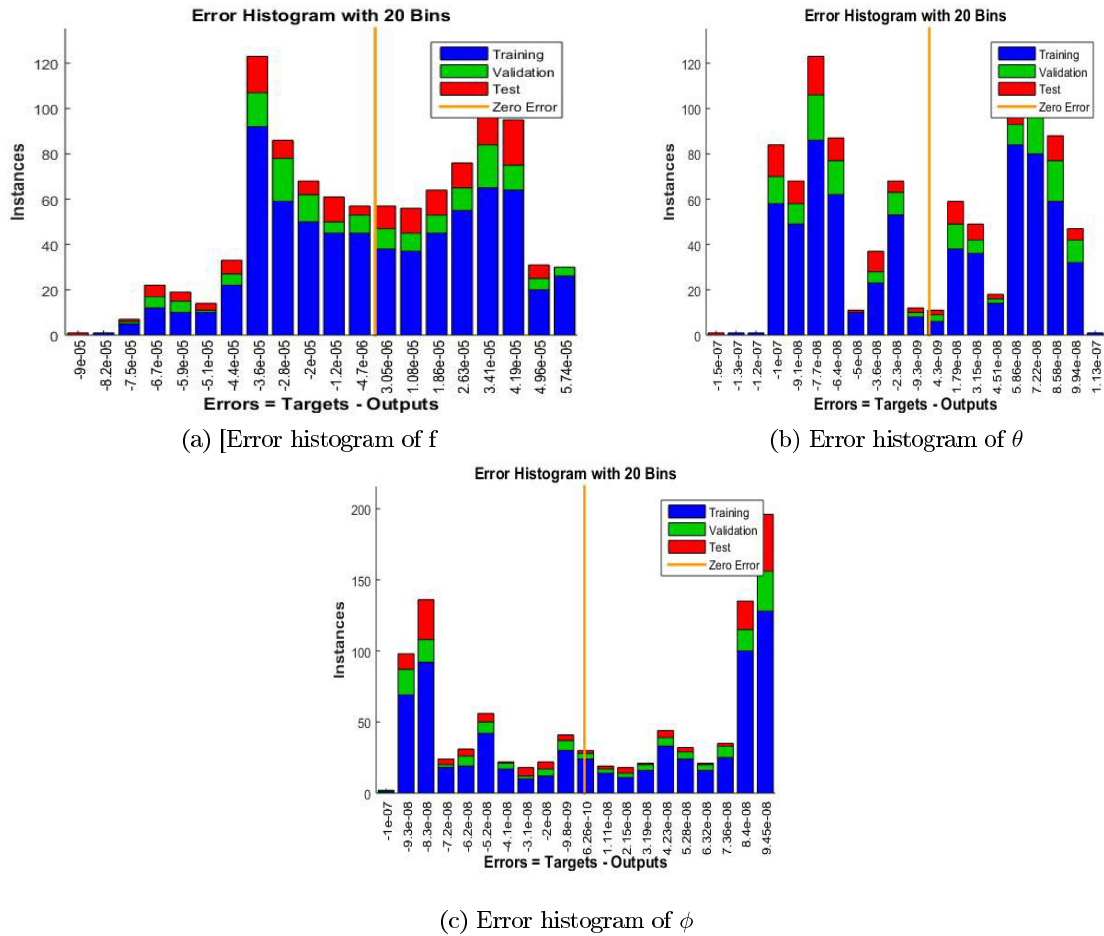
(a) [Error histogram of f

(b) Error histogram of θ

(c) Error histogram of φ

FIGURE 31. Example III: Case-C error graphs.

of case-C is given in figure 31. All variables' errors are in the range $10^{-5} - 10^{-10}$.

VI. CONCLUSION

In this article, the ocean energy generator is considered with Soret effect. The Soret effect has a significant influence on salinity of water. The transportation over an inclined surface is considered under the impact of heat production and Soret effect (thermodiffusion). The ocean energy generator consists of velocity, temperature gradient and salinity. The system is modelled mathematically. For the numerical analysis, the system is transformed into an optimisation problem. A numerical technique, NN-LMA, is designed for the optimisation pirocedure using Levenberg Marquardt algorithm and neural network (NN-LMA). Using mean square error, the fitness function is developed. The solution found by NN-LMA is evaluated with reference solution of RK4. The performance of NN-LMA is evaluated by different means, such as training, validation and testing. The evaluation results are presented graphically. The best performance of NN-LMA can be clearly observed from regression graphs.

Moreover, histograms are used to illustrate the errors. The NN-LMA algorithm consistently delivers reliable performance. The domain of NN-LMA can be extended to various physical and biological problems, allowing for investigation of its potential integration with other renewable energy technologies, such as wind or solar power, to create more efficient and sustainable hybrid systems. This may involve exploring different methods for energy storage and distribution, as well as developing new control and monitoring systems for the integrated energy systems.

ABBREVIATIONS

NN	Neural Network
ANN	Artificial neural network
AI	Artificial intelligence
Re	Local Reynolds number
Sr	Soret number
Pr	Prandtl number
α	Inclination angle
$\bar{\alpha}$	Heat source parameter
Gr	Grashof
RK4	Range-Kutta order four technique
LMA	Levenberg Marquardt algorithm

REFERENCES

[1] B. R. Hughes, N. P. S. Cherisa, and O. Beg, "Computational study of improving the efficiency of photovoltaic panels in the UAE," *World Academy Sci., Eng. Technol.*, vol. 73, pp. 278–287, Jan. 2011.

[2] R. W. Whittlesey, S. Liska, and J. O. Dabiri, "Fish schooling as a basis for vertical axis wind turbine farm design," *Bioinspiration Biomimetics*, vol. 5, no. 3, Sep. 2010, Art. no. 035005.

[3] O. A. Bég, R. Gorla, V. Prasad, B. Vasu, and R. D. Prashad, "Computational study of mixed thermal convection nanofluid flow in a porous medium," in *Proc. 12th U.K. Nat. Heat Transf. Conf.*, Sep. 2011, Paper ID 004.

[4] P. McKendry, "Energy production from biomass—Part 1: Overview of biomass," *Bioresource Technol.*, vol. 83, no. 1, pp. 37–46, May 2002.

[5] M. Kamal, M. Sulaiman, and F. S. Alshammari, "Quantitative features analysis of a model for separation of dissolved substances from a fluid flow by using a hybrid heuristic," *Eur. Phys. J. Plus*, vol. 137, no. 9, p. 1062, Sep. 2022.

[6] S. Masutani and P. Takahashi, "Ocean thermal energy conversion (OTEC)," *Oceanography*, vol. 22, no. 609, p. 625, 2001.

[7] Z. Yue, W. Zhou, and T. Li, "Impact of the Indian ocean dipole on evolution of the subsequent ENSO: Relative roles of dynamic and thermodynamic processes," *J. Climate*, vol. 34, no. 9, pp. 3591–3607, May 2021.

[8] S. Behrens, J. Hayward, M. Hemer, and P. Osman, "Assessing the wave energy converter potential for Australian coastal regions," *Renew. Energy*, vol. 43, pp. 210–217, Jul. 2012.

[9] T. F. Lin and J. B. Gilbert, "Studies of helical magnetohydrodynamic seawater flow in fields up to twelve teslas," *J. Propuls. Power*, vol. 11, no. 6, pp. 1349–1355, Nov. 1995.

[10] S. K. Ghosh, "Hydromagnetic flow in a rotating channel permeated by an inclined magnetic field in the presence of an oscillator," *Czechoslovak J. Phys.*, vol. 46, no. 1, pp. 85–95, Jan. 1996.

[11] Z. Li, K. Wang, W. Li, S. Yan, F. Chen, and S. Peng, "Analysis of surface pressure pulsation characteristics of centrifugal pump magnetic liquid sealing film," *Frontiers Energy Res.*, vol. 10, 2022, Art. no. 10:937299, doi: 10.3389/fenrg.2022.937299.

[12] Y. Peng, Z. Lin, L. Zhao, C. Sha, R. Li, Y. Xu, B. Liu, and J. Li, "Analysis of liquid metal MHD wave energy direct conversion system," in *Proc. 18th Int. Offshore Polar Eng. Conf.*, 2008, p. 448.

[13] N. A. Khan, F. S. Alshammari, C. A. T. Romero, M. Sulaiman, and S. Mirjalili, "An optimistic solver for the mathematical model of the flow of Johnson Segalman fluid on the surface of an infinitely long vertical cylinder," *Materials*, vol. 14, no. 24, p. 7798, Dec. 2021.

[14] M. Takeda, Y. Okuji, T. Akazawa, X. Liu, and T. Kiyoshi, "Fundamental studies of helical-type seawater MHD generation system," *IEEE Trans. Appiled Supercond.*, vol. 15, no. 2, pp. 2170–2173, Jun. 2005.

[15] E. Doss and G. Roy, "Flow development and analysis of MHD generators and seawater thrusters," Amer. Soc. Mech. Eng., NY, USA, Tech. Rep., 1992, doi: 10.1115/1.2910002.

[16] N. A. Khan, M. Sulaiman, P. Kumam, and A. J. Aljohani, "A new soft computing approach for studying the wire coating dynamics with Oldroyd 8-constant fluid," *Phys. Fluids*, vol. 33, no. 3, Mar. 2021, Art. no. 036117.

[17] M. Takeda, N. Tomomori, T. Akazawa, K. Nishigaki, and A. Iwata, "Flow control of seawater with a diverging duct by MHD separation method," *IEEE Trans. Trans. Supercond.*, vol. 14, no. 2, pp. 1543–1546, Jun. 2004.

[18] Q. Zhong, Y. Chen, B. Zhu, S. Liao, and K. Shi, "A temperature field reconstruction method based on acoustic thermometry," *Measurement*, vol. 200, Aug. 2022, Art. no. 111642.

[19] N. Khan, F. Ali, M. Arif, Z. Ahmad, A. Aamina, and I. Khan, "Maxwell nanofluid flow over an infinite vertical plate with ramped and isothermal wall temperature and concentration," *Math. Problems Eng.*, vol. 2021, pp. 1–19, Sep. 2021.

[20] H. Khan, F. Ali, N. Khan, I. Khan, and A. Mohamed, "Electromagnetic flow of Casson nanofluid over a vertical Riga plate with ramped wall conditions," *Frontiers Phys.*, vol. 10, p. 903, Oct. 2022.

[21] G. Srikanth, G. Srinivas, and B. Reddy, "Mhd convective heat transfer of a nanofluid flow past an inclined permeable plate with heat source and radiation," *Int. J. Phys. Math. Sci.*, vol. 3, no. 6, pp. 89–95, 2013.

[22] G. K. Ramesh, B. J. Gireesha, and C. S. Bagewadi, "Heat transfer in MHD dusty boundary layer flow over an inclined stretching sheet with non-uniform heat source/sink," *Adv. Math. Phys.*, vol. 2012, pp. 1–13, Jan. 2012.

[23] M. A. Kabir and M. A. A. Mahbub, "Effects of thermophoresis on unsteady MHD free convective heat and mass transfer along an inclined porous plate with heat generation in presence of magnetic field," *Open J. Fluid Dyn.*, vol. 2, no. 4, pp. 120–129, 2012.

[24] G. Palani and K. Y. Kim, "Joule heating and viscous dissipation effects on MHD flow past a semi-infinite inclined plate with variable surface temperature," *J. Eng. Thermophys.*, vol. 20, no. 4, pp. 501–517, Dec. 2011.

[25] B. Zhou, J. Hu, P. Jin, K. Sun, Y. Li, and D. Ning, "Power performance and motion response of a floating wind platform and multiple heaving wave energy converters hybrid system," *Energy*, vol. 265, Feb. 2023, Art. no. 126314.

[26] H. M. Ramadan and A. J. Chamkha, "Hydromagnetic free convection of a particulate suspension from a permeable inclined plate with heat absorption for non-uniform particle-phase density," *Heat Mass Transf.*, vol. 39, no. 5, pp. 367–374, Jun. 2003.

[27] C.-H. Chen, "Heat and mass transfer in MHD flow by natural convection from a permeable, inclined surface with variable wall temperature and concentration," *Acta Mechanica*, vol. 172, nos. 3–4, pp. 219–235, Nov. 2004.

[28] C.-C. Wang and C.-K. Chen, "Mixed convection boundary layer flow on inclined wavy plates including the magnetic field effect," *Int. J. Thermal Sci.*, vol. 44, no. 6, pp. 577–586, Jun. 2005.

[29] N. A. Khan, M. Sulaiman, and F. S. Alshammari, "Heat transfer analysis of an inclined longitudinal porous fin of trapezoidal, rectangular and dovetail profiles using cascade neural networks," *Struct. Multidisciplinary Optim.*, vol. 65, no. 9, p. 251, Sep. 2022.

[30] B. Gebhart, *Heat Conduction and Mass Diffusion*, vol. 634. New York, NY, USA: McGraw-Hill, 1993.

[31] M. M. Rashidi, N. Rahimzadeh, M. Ferdows, M. J. Uddin, and O. A. Bég, "Group theory and differential transform analysis of mixed convective heat and mass transfer from a horizontal surface with chemical reaction effects," *Chem. Eng. Commun.*, vol. 199, no. 8, pp. 1012–1043, Aug. 2012.

[32] M. Ferdows, M. J. Uddin, and T. S. Khaleque, "Double diffusion, slips and variable diffusivity effects on combined heat mass transfer with variable viscosity via a point transformation," *Prog. Comput. Fluid Dyn., Int. J.*, vol. 13, no. 1, pp. 54–64, 2013.

[33] J. Zueco, O. A. Bég, H. S. Takhar, and V. R. Prasad, "Thermophoretic hydromagnetic dissipative heat and mass transfer with lateral mass flux, heat source, ohmic heating and thermal conductivity effects: Network simulation numerical study," *Appl. Thermal Eng.*, vol. 29, nos. 14–15, pp. 2808–2815, Oct. 2009.

[34] S. Nasir, A. S. Berrouk, A. Aamir, and T. Gul, "Significance of chemical reactions and entropy on darcy-forchheimer flow of H_2O and $C_2H_6O_2$ convening magnetized nanoparticles," *Int. J. Thermofluids*, vol. 17, Feb. 2023, Art. no. 100265.

[35] B. Zhou, Z. Zheng, Q. Zhang, P. Jin, L. Wang, and D. Ning, "Wave attenuation and amplification by an abreast pair of floating parabolic breakwaters," *Energy*, vol. 271, May 2023, Art. no. 127077.

[36] Y. Lin, H. Song, F. Ke, W. Yan, Z. Liu, and F. Cai, "Optimal caching scheme in D2D networks with multiple robot helpers," *Comput. Commun.*, vol. 181, pp. 132–142, Jan. 2022.

[37] O. D. Makinde, K. Zimba, and O. A. Bég, "Numerical study of chemically-reacting hydromagnetic boundary layer flow with Soret/Dufour effects and a convective surface boundary condition," *Int. J. Thermal Environ. Eng.*, vol. 4, no. 1, pp. 89–98, Mar. 2012.

[38] C. R. A. Abreu, M. F. Alfradique, and A. S. Telles, "Boundary layer flows with Dufour and Soret effects: I: Forced and natural convection," *Chem. Eng. Sci.*, vol. 61, no. 13, pp. 4282–4289, Jul. 2006.

[39] M. F. Khan, M. Sulaiman, C. A. T. Romero, and F. S. Alshammari, "A quantitative study of non-linear convective heat transfer model by novel hybrid heuristic driven neural soft computing," *IEEE Access*, vol. 10, pp. 34133–34153, 2022.

[40] G. Chen, P. Chen, W. Huang, and J. Zhai, "Continuance intention mechanism of middle school student users on online learning platform based on qualitative comparative analysis method," *Math. Problems Eng.*, vol. 2022, pp. 1–12, Mar. 2022.

[41] M. F. Khan, M. Sulaiman, and F. S. Alshammari, "A hybrid heuristic-driven technique to study the dynamics of savanna ecosystem," *Stochastic Environ. Res. Risk Assessment*, vol. 37, no. 1, pp. 1–25, Jan. 2023.

[42] T. Gul, S. Mukhtar, W. Alghamdi, Z. Raizah, S. E. Alhazmi, and E. T. ElDin, "Radiative couple stress Casson hybrid nanofluid flow over an inclined stretching surface due to nonlinear convection and slip boundaries," in *Modern World Heat Transfer Problems: Role of Nanofluids and Fractional Order Approaches*, vol. 10. Lausanne, Switzerland: Frontiers, Oct. 2022, p. 212.

[43] M. F. Khan, M. Sulaiman, C. A. T. Romero, and A. Alkhathlan, "A hybrid metaheuristic based on neurocomputing for analysis of unipolar electrohydrodynamic pump flow," *Entropy*, vol. 23, no. 11, p. 1513, Nov. 2021.

[44] O. A. Bég, A. Bakier, R. Prasad, and S. K. Ghosh, "Numerical modelling of non-similar mixed convection heat and species transfer along an inclined solar energy collector surface with cross diffusion effects," *World J. Mech.*, vol. 1, no. 4, pp. 185–196, 2011.

[45] J. Xiang, L. Deng, C. Zhou, H. Zhao, J. Huang, and S. Tao, "Heat transfer performance and structural optimization of a novel micro-channel heat sink," *Chin. J. Mech. Eng.*, vol. 35, no. 1, p. 38, 2022., doi: 10.1186/s10033-022-00704-5.

[46] N. A. Khan, M. Sulaiman, E. Bonyah, J. Seidu, and F. S. Alshammari, "Investigation of three-dimensional condensation film problem over an inclined rotating disk using a nonlinear autoregressive exogenous model," *Comput. Intell. Neurosci.*, vol. 2022, pp. 1–12, Feb. 2022.

[47] F. Ali, F. Haq, N. Khan, H. Alqahtani, A. Imtiaz, and I. Khan, "A report of generalized blood flow model with heat conduction between blood and particles," *J. Magn.*, vol. 27, no. 2, pp. 186–200, Jun. 2022.

[48] F. Ali, F. Haq, N. Khan, A. Imtiaz, and I. Khan, "A time fractional model of hemodynamic two-phase flow with heat conduction between blood and particles: Applications in health science," *Waves Random Complex Media*, vol. 38, pp. 1–28, Jul. 2022.

[49] O. A. Bég and D. Tripathi, "Mathematica simulation of peristaltic pumping with double-diffusive convection in nanofluids: A bio-nano-engineering model," *Proc. Inst. Mech. Eng., N, J. Nano. Nanosyst.*, vol. 225, no. 3, pp. 99–114, Sep. 2011.

[50] J. Xiang, W. Yang, H. Liao, P. Li, Z. Chen, and J. Huang, "Design and thermal performance of thermal diode based on the asymmetric flow resistance in vapor channel," *Int. J. Thermal Sci.*, vol. 191, Sep. 2023, Art. no. 108345.

[51] L. Sun, J. Hou, C. Xing, and Z. Fang, "A robust Hammerstein–Wiener model identification method for highly nonlinear systems," *Processes*, vol. 10, no. 12, p. 2664, Dec. 2022.

[52] S. Murtaza, P. Kumam, A. Kaewkhao, N. Khan, and Z. Ahmad, "Fractal fractional analysis of non linear electro osmotic flow with cadmium telluride nanoparticles," *Sci. Rep.*, vol. 12, no. 1, Nov. 2022, Art. no. 20226.

[53] Q. Xu, C. Shang, H. Ma, Q. Hong, C. Li, S. Ding, L. Xue, X. Sun, Y. Pan, T. Sugahara, Y. Yalikun, Y.-C. Lai, and Y. Yang, "A guided-liquid-based hybrid triboelectric nanogenerator for omnidirectional and high-performance ocean wave energy harvesting," *Nano Energy*, vol. 109, May 2023, Art. no. 108240.

[54] R. M. L. Coelho and A. S. Telles, "Extended graetz problem accompanied by Dufour and soret effects," *Int. J. Heat Mass Transf.*, vol. 45, no. 15, pp. 3101–3110, Jul. 2002.

[55] O. A. Bég, A. Y. Bakier, and V. R. Prasad, "Numerical study of free convection magnetohydrodynamic heat and mass transfer from a stretching surface to a saturated porous medium with Soret and Dufour effects," *Comput. Mater. Sci.*, vol. 46, no. 1, pp. 57–65, Jul. 2009.

[56] T. Gul, M. Z. Ullah, A. K. Alzahrani, and I. S. Amiri, "Thermal performance of the graphene oxide nanofluids flow in an upright channel through a permeable medium," *IEEE Access*, vol. 7, pp. 102345–102355, 2019.

[57] O. Bég, R. Bhargava, S. Rawat, and E. Kahya, "Numerical study of micropolar convective heat and mass transfer in a non-Darcy porous regime with Soret and Dufour diffusion effects," *Emirates J. Eng. Res.*, vol. 13, no. 2, pp. 51–66, 2008.

[58] B. Vasu, O. A. Bég, N. Reddy, and V. Prasad, "Thermo-diffusion and diffusion-thermo effects on free convection flow past a semi-infinite vertical plate in the presence of suction and injection," *Int. J. Energy Tech.*, vol. 14, no. 5, pp. 1–11, 2013.

[59] G. Yao, Z. Luo, Z. Lu, M. Wang, J. Shang, and J. M. Guerrerob, "Principle and control strategy of a novel wave-to-wire system embedded ocean energy storage optimization," *Ocean Eng.*, vol. 271, Mar. 2023, Art. no. 113762.

[60] R. N. Silva, M. M. Nunes, F. L. Oliveira, T. F. Oliveira, A. C. P. Brasil, and M. S. S. Pinto, "Dynamical analysis of a novel hybrid oceanic tidal-wave energy converter system," *Energy*, vol. 263, Jan. 2023, Art. no. 125933.

[61] K. Nonlaopon, M. F. Khan, M. Sulaiman, F. S. Alshammari, and G. Laouini, "Analysis of MHD Falkner–Skan boundary layer flow and heat transfer due to symmetric dynamic wedge: A numerical study via the SCA-SQP-ANN technique," *Symmetry*, vol. 14, no. 10, p. 2180, Oct. 2022.

[62] M. A. Boyacioglu, Y. Kara, and Ö. K. Baykan, "Predicting bank financial failures using neural networks, support vector machines and multivariate statistical methods: A comparative analysis in the sample of savings deposit insurance fund (SDIF) transferred banks in Turkey," *Expert Syst. Appl.*, vol. 36, no. 2, pp. 3355–3366, Mar. 2009.

[63] M. Fawad Khan, E. Bonyah, F. S. Alshammari, S. M. Ghufran, and M. Sulaiman, "Modelling and analysis of virotherapy of cancer using an efficient hybrid soft computing procedure," *Complexity*, vol. 2022, pp. 1–29, Jan. 2022.

[64] S. Haykin and N. Network, "A comprehensive foundation," *Neural Netw.*, vol. 2, p. 41, Feb. 2004.

[65] H. Rahmanifard and T. Plaksina, "Application of artificial intelligence techniques in the petroleum industry: A review," *Artif. Intell. Rev.*, vol. 52, no. 4, pp. 2295–2318, Dec. 2019.

[66] V. S. Dave and K. Dutta, "Neural network based models for software effort estimation: A review," *Artif. Intell. Rev.*, vol. 42, no. 2, pp. 295–307, Aug. 2014.

[67] H. He and E. A. Garcia, "Learning from imbalanced data," *IEEE Trans. Knowl. Data Eng.*, vol. 21, no. 9, pp. 1263–1284, Sep. 2009.

[68] A. Mozaffari, M. Emami, and A. Fathi, "A comprehensive investigation into the performance, robustness, scalability and convergence of chaos-enhanced evolutionary algorithms with boundary constraints," *Artif. Intell. Rev.*, vol. 52, no. 4, pp. 2319–2380, Dec. 2019.

[69] N. Izeboudjen, C. Larbes, and A. Farah, "A new classification approach for neural networks hardware: From standards chips to embedded systems on chip," *Artif. Intell. Rev.*, vol. 41, no. 4, pp. 491–534, Apr. 2014.

[70] D. Wang, H. He, and D. Liu, "Intelligent optimal control with critic learning for a nonlinear overhead crane system," *IEEE Trans. Ind. Informat.*, vol. 14, no. 7, pp. 2932–2940, Jul. 2018.

• • •